NACA

RESEARCH MEMORANDUM

AERODYNAMIC AND HYDRODYNAMIC CHARACTERISTICS OF A PROPOSED

SUPERSONIC MULTIJET WATER-BASED HYDRO-SKI AIRCRAFT

WITH A VARIABLE-INCIDENCE WING

By William W. Petynia, Dennis F. Hasson,
and Stanley H. Spooner

Langley Aeronautical Laboratory
Langley Field, Va.

CLASSIFIED DOCUMENT

This material contains information affecting the National Defense of the United States within the meaning of the espionage laws, Title 18, U.S.C., Secs. 793 and 794, the transmission or revelation of which in any manner to an unauthorized person is prohibited by law.

NATIONAL ADVISORY COMMITTEE
FOR AERONAUTICS
WASHINGTON
October 23, 1957

NATIONAL ADVISORY COMMITTEE FOR AERONAUTICS

RESEARCH MEMORANDUM

AERODYNAMIC AND HYDRODYNAMIC CHARACTERISTICS OF A PROPOSED

SUPERSONIC MULTIJET WATER-BASED HYDRO-SKI AIRCRAFT

WITH A VARIABLE-INCIDENCE WING

By William W. Petynia, Dennis F. Hasson,
and Stanley H. Spooner

SUMMARY

An investigation has been conducted to determine the aerodynamic and hydrodynamic characteristics of a supersonic multijet water-based bomber. The aircraft utilized a retractable hydro-ski, tiltable engine-wing arrangement, high fineness ratio, low frontal area, and supersonic area treatment. The wing had an unswept 80-percent-chord line, an aspect ratio of 3.5, a taper ratio of 0.067, and 3-percent-thick airfoil sections. The Mach number range of the aerodynamic tests was 0.6 to 1.97.

The minimum aerodynamic drag coefficient remained nearly constant in the supersonic speed range and was approximately 1.7 times the subsonic drag level. No appreciable longitudinal destabilizing tendencies were encountered throughout the lift and Mach number ranges. A stable variation in the lateral and directional stability parameters was obtained throughout the supersonic speed range.

Longitudinal stability during take-offs and landings was satisfactory and sufficient excess thrust was available for acceleration to take-off. The inlets were free from spray throughout the take-off for all gross loads investigated.

INTRODUCTION

The subject investigation is part of the high-speed-seaplane research program undertaken at the Langley Laboratory in cooperation with the Bureau of Aeronautics, Department of the Navy, and the aircraft industry to investigate the performance capabilities of water-based aircraft. In this program the Bureau of Aeronautics has suggested mission requirements, while the aircraft manufacturers have contributed design ideas compatible with manufacturing feasibility. The National Advisory Committee for

Aeronautics has assumed the technical supervision and responsibility for the overall layout and the selection of the configurations.

The aerodynamic and hydrodynamic characteristics have been obtained for a series of designs based on various requirements (refs. 1 to 5). These configurations have offered a variety of design solutions to the problems associated with high-speed water-based aircraft. The results of these studies, together with recent advances in aerodynamic knowledge and progress in engine design, indicated that a configuration with increased speed capabilities and sufficient range to meet a Navy mission requirement of a Mach 2 dash and a 1,500-nautical-mile combat radius could be designed. The configuration described in this paper represents one approach to such an airplane and the results of the wind-tunnel and tank evaluations are presented.

In the present investigation, the aerodynamic longitudinal charac- teristics over a Mach number range from 0.6 to 1.97 were obtained. In addition, the lateral characteristics were obtained in the supersonic Mach number range (1.56 to 1.97). The hydrodynamic investigation in smooth water included take-off resistance, longitudinal stability during take-offs and landings, and spray characteristics.

<div align="center">SYMBOLS</div>

All aerodynamic data have been reduced to standard nondimensional coefficients. The wind-tunnel data are referred to the stability-axes system (fig. 4) with the axes originating in the model plane of symmetry at 35 percent of the mean aerodynamic chord in the wing-chord plane and 26.6 percent of the mean aerodynamic chord above the fuselage base line.

All hydrodynamic data as presented have been converted to the full- size values. The center of gravity was located at 25 percent of the mean aerodynamic chord in the wing-chord plane and 26.6 percent of the mean aerodynamic chord above the fuselage base line.

<div align="center">Aerodynamic</div>

C_L lift coefficient, $\dfrac{\text{Lift}}{qS}$

C_D drag coefficient, $\dfrac{\text{Drag}}{qS}$

$C_{D,i}$ internal-drag coefficient per duct based on wing area

C_m pitching-moment coefficient, $\dfrac{\text{Pitching moment}}{qS\bar{c}}$

$C_{l,s}$ rolling-moment coefficient, referred to stability axes, $\dfrac{\text{Rolling moment}}{qSb}$

$C_{n,w}$ yawing-moment coefficient, referred to wind axes, $\dfrac{\text{Yawing moment}}{qSb}$

C_Y side-force coefficient, $\dfrac{\text{Side force}}{qS}$

M free-stream Mach number

L/D lift-drag ratio, C_L/C_D

m mass-flow rate, slugs/sec

q free-stream dynamic pressure, lb/sq ft

S wing area, sq ft

$\bar{c}$ wing mean aerodynamic chord, ft

b wing span, ft

ρ air density, slugs/cu ft

A_i duct capture area, sq ft

V free-stream velocity, ft/sec

α angle of attack of wing-chord plane, deg

β angle of sideslip, deg

ϕ angle of roll, deg

i_t angle of incidence of horizontal tail, referred to wing-chord plane when wing incidence is at $2.5°$, deg

C_{L_α} lift-curve slope, measured at zero lift, per deg

$C_{m_{C_L}}$ pitching-moment-curve slope, $(C_m \approx 0)$

$C_{m_{i_t}}$ rate of change of pitching-moment coefficient with tail incidence per deg

C_{l_β} rate of change of rolling-moment coefficient with sideslip angle, $\dfrac{\partial C_{l,s}}{\partial \beta}$

C_{n_β} rate of change of yawing-moment coefficient with sideslip angle, $\dfrac{\partial C_{n,w}}{\partial \beta}$

C_{Y_β} rate of change of side-force coefficient with sideslip angle, $\dfrac{\partial C_Y}{\partial \beta}$

Subscripts:

min   minimum

max   maximum

Hydrodynamic

b   hydro-ski beam, ft

C_{Δ_0} gross-load coefficient, Δ_0 / wb^3

L.W.L.   load water line

w   specific weight of water (63.3 lb/cu ft for these tests)

Δ_0 gross load, lb

τ trim, angle between fuselage base line and horizontal, deg

δ_e elevator deflection referred to stabilizer chord, positive when trailing edge is down

δ_s stabilizer incidence referred to fuselage base line, positive when trailing edge is down

r   rise, height of trailing edge of hydro-ski above free-water surface when trim is zero, ft

R   total resistance (including air drag), lb

DESIGN OF CONFIGURATION

Preliminary Considerations

The mission considered for this design required that the aircraft cruise at a high subsonic speed to and from the target area and be capable of a Mach 2 dash while subject to interception. A combat radius in the order of 1,500 nautical miles was desired.

A variety of wing-body and engine arrangements were studied to determine the layout most promising from aerodynamic and hydrodynamic considerations. Careful consideration was given to the weight, location, and structural requirements of the components.

Preliminary performance estimates and range calculations, based on estimated lift-drag ratios and engine performance, indicated that the mission could be accomplished by an aircraft with a rather high wing loading and a large fuel load. Efficient internal arrangement of the fuel load and components is essential to obtain the minimum volume and skin area.

The resulting configuration inherently has reduced spray clearances. A hydro-ski, extended below the fuselage, would provide additional clearances after emergence and could be retracted into the fuselage to produce a clean configuration for the flight condition. The added weight of the ski and retracting mechanism should be offset by a lower aerodynamic drag or a lighter fuselage structural weight when compared with an equivalent hull-type configuration with chines and step.

A general arrangement of the configuration is shown in figure 1 and a layout of the fuselage is shown in figure 2. The pertinent characteristics and dimensions are given in table I.

Description of Components

Engines and nacelles.- Four turbojet engines, advanced versions of the Orenda Iroquois PS-13 with afterburners, producing a combined maximum sea-level thrust of 126,000 pounds, were used.

The two forward engines were in pods located ahead of and below the wing, and were favorable for the area-rule considerations and for aerodynamic interferences. The two rear engines were mounted in a single nacelle on the vertical tail for a favorable inlet location for spray clearances and reduced the length of ducting required. A variable-geometry spike inlet, as described in reference 6, was used on the forward engines and a common inlet of the external compression-ramp type

with a splitter plate was used for the two engines in the rear nacelle (ref. 7).

Aerodynamic surfaces.- The wing had zero sweep angle measured at the 80-percent-chord location and an NACA 65A003 airfoil section parallel to the line of symmetry. The wing aspect ratio was 3.5 with a taper ratio of 0.067 and no twist was incorporated. The horizontal tail was a delta plan form with a leading-edge sweep angle of 45° and an NACA 65A004 airfoil section. The wing-tail combination was selected on the basis of extensive stability research in the Langley high-speed 7- by 10-foot tunnel (ref. 8). The horizontal-tail position and height were selected to provide aerodynamic stability while maintaining adequate spray clearances.

The small span and thickness of the wing, together with the forward engine location, made it difficult to locate effectively the conventional high-lift devices necessary for reducing the take-off and landing speeds. It appeared practical to vary the wing incidence for increased lift at landing and take-off. An additional advantage would be to rotate the wing about the trailing edge to lift the forward nacelles clear of spray. The mechanism necessary for rotation could be located within the fuselage. The wing was therefore rotated about a point on the fuselage center line behind the wing trailing edge. With the wing rotated 10°, take-off and landing speeds would be in the order of 200 knots for a gross-load condition of 225,000 pounds (wing loading of 150 pounds per square foot). Further speed reductions could be made by the application of recent developments in high-lift devices (ref. 9).

Hydrodynamic surfaces.- A single ski with an area of 215 square feet was located with the trailing edge 11.7 feet below the fuselage and 0.6 foot forward of $\bar{c}/4$. (See fig. 1.) The ski incidence was 2° referred to the base line of the fuselage. The ski area was determined for the hydrodynamic take-off resistance in smooth water, although the application of a variable-area ski to effect a high beam loading would result in a large reduction of the landing impacts (ref. 10).

The center section of the ski conformed to the fuselage in cross section in the region of the retracted position. Two outboard flat sections that could be hinged upward to produce a higher beam loading had an angle of dead rise of -10°. When the outer panels were in the extended position, the ski was assumed to have a 0° dead-rise angle and the data presented in reference 11 for a flat plate were used for computations to determine the area and size.

An aerodynamically clean forebody was used without chines or chine strips. A V-bottom planing surface with a 20° angle of dead rise was faired into the afterbody. The angles of the afterbody keel and chines to the forebody keel were kept small so that they would follow as nearly as possible the stream flow lines.

Because of the height and small tip chord of the thin wing, conventional wing-tip floats could not be efficiently located on this configuration. In addition, tip floats have been shown in reference 1 to contribute appreciably to the aerodynamic drag. A retractable auxiliary device to provide transverse stability was assumed.

Area Curve

The total cross-sectional-area curve for a Mach number of 1.4 and the contribution of the various components are shown in figure 3. The method for obtaining the supersonic area distribution was similar to that used in references 12 and 13. The small wing and longitudinal distribution of the components not only resulted in a low maximum cross-sectional area (107 square feet) but also provided a smooth longitudinal distribution of this cross-sectional area with minimum fuselage indentation.

MODELS

Wind Tunnel

Photographs of the 1/42.5-size wind-tunnel model are presented in figure 5. The same wind-tunnel model and strain-gage balance were used for the transonic and supersonic tests. The wing, the pylon-mounted nacelles, and the tail surfaces were constructed of stainless steel. The tail-mounted nacelles were of plastic and Fiberglas-cloth construction. The hull was of plastic and Fiberglas cloth over a steel core.

The rear portion of the hull was cut off to allow installation of the support sting.

Tank

Photographs of the 1/20-size dynamic model used for the hydrodynamic investigation are presented in figure 6. The model was constructed of plastic-impregnated Fiberglas and wood. The hydro-ski struts were circular arcs in cross section and were made of aluminum. Leading-edge slats were used to prevent premature wing stall that usually is encountered at the low Reynolds numbers of tank tests.

Thrust for the two forward engines was simulated by compressed-air motors. Air was supplied to the model by a 3/8-inch flexible plastic tubing from a high-pressure air supply on the towing carriage.

Electric contacts were located on the keel at the bow, sternpost, and trailing edge of the hydro-ski to indicate when these portions of the model were in the water. These electric contacts also were used to release the trim brake during the landing tests.

APPARATUS AND TESTS

Wind Tunnels

The aerodynamic tests of the model were conducted in the Langley 8-foot transonic pressure tunnel and the Langley Unitary Plan wind tunnel. The forces and moments on the sting-supported model were measured simultaneously by means of an electrical strain-gage balance mounted within the model. The angle of attack was measured by means of an electrical strain-gage pendulum device mounted internally at the base of the support sting. The mass-flow ratios and the internal-drag coefficients were determined by means of pressure orifices located within the engine ducts. A static-pressure orifice was also provided to determine the base pressure at the aft end of the hull.

Tests were made at transonic and supersonic speeds of the complete model configuration with a wing incidence of 2.5°, a horizontal-tail incidence of -2.5°, and natural transition. Additional tests at transonic speeds which included horizontal-tail off and horizontal-tail incidences of -2.5° and -12.5° were conducted with fixed transition. The transition was fixed by means of No. 120 carborundum grains attached in a 0.1-inch-wide strip at 10 percent of the local chord behind the leading edge of all airfoil surfaces. Similar strips were attached at approximately 5 percent of the respective lengths behind the upstream end of the hull, the pylon-mounted nacelles, and the tail-mounted nacelles. The additional configurations investigated at supersonic speeds consisted of the model with various combinations of the horizontal tail at incidences of -2.5° and -12.5°, vertical tails, and the tail nacelle. A few tests were made with transition fixed on the wing and fuselage of the model. For these tests transition strips were placed around the fuselage 3 inches aft of the nose and along the 10-percent-chord line of the upper and lower surfaces of the wing. The strips were 1/4-inch wide and consisted of No. 70 carborundum grains attached with shellac.

The test conditions for the transonic and supersonic wind-tunnel tests were:

	8-foot transonic pressure tunnel	Unitary Plan wind tunnel
Stagnation pressure, atm	0.47, 1.0	0.68
Stagnation temperature, °F	124	125
Dew point, °F	<0	<-30
Mach number	0.6 to 1.2	1.56, 1.77, 1.97
Yaw angle, deg	0	-4 to 11
Angle of attack, deg	-2 to 13	-4 to 12
Wing incidence, deg	2.5	2.5
Horizontal-tail incidence, deg . .	-2.5, -12.5	-2.5, -12.5

The variation of Reynolds number based on $\bar{c}$ with Mach number is shown in figure 7.

Tank

The hydrodynamic investigation was made in the Langley tank no. 1, which is described in reference 14. The apparatus and procedure used to investigate the hydrodynamic characteristics of dynamic models (ref. 15) are similar to those used for this investigation. A photograph of the setup of the model and the towing apparatus is presented in figure 8.

A wing incidence of 10° with the center of gravity located at $0.25\bar{c}$ was used for the hydrodynamic evaluation. The horizontal stabilizer and elevators could be fixed at angles of 5° to -15° and 20° to -20°, respectively. The model was free to trim about the center of gravity and to move vertically but was restrained laterally and in roll and yaw. For the landing investigation, the model was fixed in trim at the landing trim and released upon contact with the water surface to permit freedom in trim and rise. Slide-wire pickups were used to obtain records of the trim and rise.

The resistance of the complete model, including air drag, was determined at constant speeds for a range of tail settings at speeds up to take-off. The thrust moments of the four engines were simulated by a static moment and the load was corrected for the vertical component of the thrust by reducing the gross weight.

During the tests with power, scale thrust for the forward engines was approximated by the air motors. The thrust moment and lift forces of the rear engines were simulated as before. Pictures and observations were made of the spray patterns during these runs.

The landings and take-offs were made at a weight corresponding to the design gross load of 225,000 pounds. The maximum constant acceleration available from the towing carriage (approximately 5 ft/sec²) was

used for the take-offs. This acceleration was less than the calculated
acceleration based on the excess thrust determined from the constant-
speed resistance tests.

CORRECTIONS AND ACCURACY

Wind Tunnels

Corrections.- The drag data have been adjusted in such a way that
the hull and nacelle base pressures correspond to the condition of free-
stream static pressure. In addition, the internal drag has been subtracted
from the drag data to give a net external drag.

Corrections for the effect of balance and sting deflection due to
load have been applied to the angle of attack and to the angle of sideslip.

Blockage corrections in the Langley 8-foot transonic pressure tunnel
are negligible and have not been applied to the data. At the Mach numbers
for which the transonic data are presented, the effects of the boundary-
reflected disturbances are generally negligible. At a Mach number of 1.15,
however, the drag results appear questionable. Although schlieren photo-
graphs indicated that the boundary-reflected disturbances pass downstream
of the model, the drag results at this Mach number may be influenced by
disturbances feeding upstream through the sting boundary layer.

For the tests in the Langley Unitary Plan wind tunnel, no correc-
tions have been applied to the data for stream angularity or buoyancy,
inasmuch as the calibration of the test section has been only partially
completed. Preliminary indications are that both the flow angularity
and the longitudinal pressure gradients are negligible.

Accuracy.- The estimated accuracy of the angles of attack and side-
slip and the coefficients, based on balance calibration and repeatability
of the data, is within the following limits:

	8-foot transonic pressure tunnel	Unitary Plan wind tunnel
Mach number	±0.003	±0.015
α, deg	±0.1	±0.1
β, deg	------	±0.1
C_L	±0.004	±0.01
C_D	±0.001	±0.001
C_m	±0.004	±0.002
$C_{l,s}$	------	±0.0005
$C_{n,w}$	------	±0.0005
C_Y	------	±0.0025

Tank

Corrections.- The resistance data presented are the net resistance with the drag of the towing staff and power leads subtracted as a tare from the total resistance.

Accuracy.- The accuracy of the measurements of the model is believed to be within the following limits:

Resistance, lb . . . . ±0.1
Trim, deg . . . . ±0.1
Speed, fps . . . . ±0.1

RESULTS AND DISCUSSION

Aerodynamic

The variation of internal-drag coefficient of the pylon-mounted nacelles and the tail-mounted nacelles with Mach number is presented in figure 9. The sum of these values is the magnitude of the correction which has been applied to the basic drag data to obtain the net external-drag coefficient. The inlet mass-flow ratios also are presented in figure 9. These ratios throughout the speed range are somewhat less than the design ratio of 0.90.

Schlieren photographs for the complete model are presented in figure 10 for Mach numbers of 1.56, 1.77, and 1.97.

Longitudinal characteristics.- The basic longitudinal aerodynamic data for the test speed range are presented in figures 11 to 17. The longitudinal characteristics for the model throughout the Mach number range are summarized in figures 18, 19, and 20.

No pitch-up tendencies were observed throughout the lift-coefficient range and Mach number range of these tests for the complete model configuration (see figs. 11, 13, 14, 15, and 16).

The variation through the Mach number range 0.60 to 1.97 of the static longitudinal-stability parameter $C_{m_{C_L}}$, measured at $C_m \approx 0$, is presented in figure 18 for the complete model with a horizontal-tail incidence of -2.5° and natural transition. The variation of $C_{m_{C_L}}$ with Mach number for the horizontal-tail-off configuration with fixed transition is also included in figure 18 for comparison since it was found that fixing transition on the model had a negligible effect on the static stability characteristics (see figs. 11 and 13). The data for the supersonic

speed range for the horizontal-tail-off configuration are not shown since the tail-mounted nacelles were also off for this configuration. The maximum rearward movement of the aerodynamic-center location is 17 percent of the mean aerodynamic chord in the transonic speed range and is followed by a gradual forward movement of the aerodynamic-center location at the higher Mach numbers.

The variation of the horizontal-tail effectiveness $C_{m_{i_t}}$ with Mach number is shown in figure 18. The horizontal-tail effectiveness reached a maximum value at a Mach number of about 0.9 and then gradually decreased in effectiveness up to a Mach number of 1.97. Horizontal-tail effectiveness, however, was maintained throughout the test Mach number range.

The variation of lift-curve slope C_{L_α} through the Mach number range of 0.6 to 1.97 is presented in figure 18 for the complete model with a horizontal-tail incidence of -2.5° and natural transition. This variation follows the usual trend through the transonic to supersonic speed range. Fixing transition was seen to have a negligible effect on the lift-curve slope (see figs. 11, 13, and 17). The variation of C_{L_α} with Mach number up to $M = 1.20$ for the configuration with horizontal tail off and fixed transition is presented (fig. 18) for comparison purposes.

The variation of minimum drag coefficient with Mach number is shown in figure 19 for the complete model with a horizontal-tail incidence of -2.5°. No attempt was made to fair the data in the Mach number range from 1.03 to 1.20 because of the questionable nature of the drag measurements obtained at $M = 1.15$. The transonic drag rise is abrupt and occurs at about $M = 0.94$. The value of $C_{D_{min}}$ with natural transition is about 0.019 at $M = 0.80$ and about 0.036 throughout the supersonic range of the investigation. With transition fixed, the value of $C_{D_{min}}$ was approximately 0.0223 at $M = 0.80$ and compares with a calculated skin-friction drag coefficient of 0.0216 (based on wing area). This value of the estimated skin-friction drag coefficient was calculated on the basis of turbulent flow and equivalent flat-plate wetted area of the various components of the configuration. At $M = 1.20$, with transition fixed, a value of $C_{D_{min}}$ of 0.0382, which is only slightly higher than the value observed with natural transition, was obtained. This value represents an increase of 1.7 times the subsonic minimum drag coefficient with transition fixed.

The variation of the untrimmed maximum lift-drag ratio with Mach number is presented in figure 20 for the complete model with a horizontal-tail incidence of -2.5° and natural transition. The largest value of maximum lift-drag ratio was about 8.7 at a Mach number of 0.95 and decreased to a value of 4.28 at a Mach number of 1.97. Values of trimmed

maximum lift-drag ratio at Mach numbers of 1.56, 1.77, and 1.97 are also presented. These values were obtained by considering that the increment in pitching-moment coefficient due to change in stabilizer position varied in a linear manner with stabilizer deflection and also that the drag had a linear variation with stabilizer deflection. The results indicate that the trimmed maximum lift-drag ratio is about 4.5 at M = 1.56 and decreases to 4.0 at M = 1.97.

Lateral characteristics.- The lateral stability characteristics at Mach numbers of 1.56, 1.77, and 1.97 are presented in figure 21. The lateral stability parameters are summarized in figure 22. The complete model has positive effective dihedral $\left(-C_{l_\beta}\right)$ at angles of attack of approximately 5° and 11° throughout the test speed range. It has been found (ref. 16) that models with the wing in a high position on the fuselage have a higher degree of positive dihedral than models with the wings in a mid or low position. The vertical tail increases the effective dihedral of the model by as much as $\Delta C_{l_\beta} = -0.0024$ at low angles of attack at the lowest Mach number.

The directional stability parameter C_{n_β} shows the usual decrease with increasing Mach number at supersonic speeds. The reduction in C_{n_β} with Mach number is due largely to the reduction in lift-curve slope of the vertical tail that occurs with increasing Mach number at supersonic speeds. The directional instability of the wing-fuselage combination varies only slightly with Mach number but does increase with angle of attack. The directional stability of the complete model shows some reduction with increase in angle of attack because of the increased instability of the wing-fuselage combination although the contribution of the vertical tail to directional stability (fig. 22) increases somewhat with angle of attack. The vertical-tail nacelle shows very little effect on the directional stability properties of the model.

Hydrodynamic

Spray characteristics.- Photographs of the spray at the normal gross load of 225,000 pounds with power off are shown in figure 23. At speeds up to emergence of the hydro-ski (55 knots), the wing was clear of spray but flow was observed to cling to the smooth, rounded sides of the forebody. In this range, the afterbody sides also were wetted above the sharp chines as a result of the deep static submergence of the chines. The sharp increase in trim and rise at emergence caused the flow to break clear from both the forebody and afterbody sides.

Photographs of the spray of the normal gross load with power on are presented in figure 24. At speeds below emergence, power had no significant effect on the flow on the forebody sides but entrained and accelerated

the spray in the path of the engine exhausts. After emergence no appreciable difference was observed in the spray with power on from that with the power off.

Photographs of the spray at the maximum-overload condition (300,000 pounds) with power off is shown in figure 25. Before emergence the flow up the forebody and afterbody sides was higher and, on the under side of the wing, the flow was heavier than that for the normal gross load with power off. After emergence the spray was heavier than that for the normal gross load but did not appear excessive. Although it did not appear necessary, some control of this spray (with a possible reduction in resistance) could be obtained through the use of spray strips. Investigation of further increases in gross load was not attempted, since bow clearance was becoming impractically small. The engine inlets and horizontal tail were clear of spray throughout the speed range for all the gross loads investigated.

Resistance.- The total resistance and trim with power off are presented in figure 26. The results obtained with the hydro-ski removed to represent a retracted position are compared with results for the hydro-ski extended. With the hydro-ski in the retracted position, the increase in resistance with speed is similar to that of a displacement-type hull. Up to emergence speed, the resistance with the hydro-ski extended increases at a greater rate than with the hydro-ski retracted. This difference increases with speed and can be attributed primarily to the resistance of the submerged hydro-ski and strut. At low speeds the angle of attack of the hydro-ski was very nearly zero and contributed little lift. At approximately 20 knots the trim increased so that the hydro-ski contributed lift and a positive nose-up moment. At approximately 55 knots the lift of the hydro-ski was sufficient to produce emergence. The resulting rapid increase in trim and rise resulted in a large decrease in resistance.

The effect of variation in gross load on the resistance, trim, and rise is shown in figure 27. At rest the draft increased with load, but load had no appreciable effect on the static trim. Gross load had relatively little effect on emergence trim or speed over the range of load investigated. The maximum resistance occurred at the emergence speed for all gross loads, and the gross-load—resistance ratio at emergence did not decrease with increase in gross load. The minimum gross-load—resistance ratio varied from 2.2 for 175,000 pounds to 2.8 for 300,000 pounds. After emergence, the effect of increase in gross load on the resistance was similar to that at the resistance hump in that the increase in resistance was approximately proportional to the increase in gross load. A stable small-amplitude oscillation in trim was noted for both tail settings and is represented by the cross-hatching on the trim curve.

Excess thrust was available for acceleration to take-off for all loads investigated. The calculated take-off time and distance based upon excess thrust for a design gross load of 225,000 pounds were 30 seconds and 6,000 feet. The absence of flaps simplified the resistance problems and also the take-off procedures, since resistance usually encountered by spray striking the flaps was eliminated. If flaps were used, there appears to be adequate spray clearance after the spray from the hydro-ski clears the wing (approximately 120 knots).

The effect of power on resistance is presented in figure 28. At speeds up to emergence, an increase in the resistance with power is noted. This increase in resistance was probably caused by the increased velocity of the spray in the path of the engine exhausts striking the model. Power also is seen to produce a slight reduction in the trim for this speed range. Above the emergence speed, with the afterbody clear of spray, power has little effect on resistance or trim.

The variation in resistance, trim, and rise with stabilizer-elevator deflection for the normal gross load is shown in figure 29; also shown is the minimum trim at which the hydro-ski will support the load on the water at a given speed. The minimum-trim curve was estimated from measurements of the aerodynamic lift of the model and estimates of the ski lift from the planing-surface data of reference 11.

The tail setting had little effect upon the trim up to a speed of 85 knots. For speeds greater than 85 knots, a wide range of stable trims is available.

Take-off stability.- Variations in trim and rise during accelerated take-offs are presented in figure 30 for a normal gross load of 225,000 pounds and several stabilizer-elevator deflections. At speeds below 85 knots, the trim was not affected by the tail setting. Between 90 and 130 knots, an oscillation in trim was noted for all of the tail settings. The model trimmed about the trailing edge of the hydro-ski, the afterbody rising clear and transferring all the water load to the hydro-ski, then falling to plane on the hydro-ski wake. Because of the low aerodynamic damping of this configuration, the trim oscillation was largely limited by the positive hydrodynamic moment provided by the increased wetted length of the hydro-ski as the model trimmed down and by the negative hydrodynamic moment of the afterbody planing forces as the model trimmed up.

With the stabilizer-elevator deflection for a maximum positive moment, there was an indication of an upper trim limit of stability near the take-off speed. This instability which occurred at high trims does not appear to be a take-off problem since the motions were not violent and the maximum amplitude of the oscillation did not exceed 4°.

Landing stability.- Smooth-water landings were made over a range of landing trims from 8° to 14°, at a gross load of 225,000 pounds. The variations in trim and rise for two typical landings at trims above and below the sternpost angle are presented in figure 31. All the landings were stable, although damped oscillations in trim and rise were encountered. The motions of the model during landing were similar for all landing trims, and the trim at contact therefore had no significant effect upon the landing behavior.

Recent preliminary free-launch catapult tests with the outboard sections of the hydro-ski hinged upward indicated sizable reductions in the landing impacts in both smooth and rough water over that with the sides extended. No stability problems were encountered during the preliminary investigation. The afterbody planing surface and a reduced sternpost angle were effective in reducing the motions resulting from wave impacts.

CONCLUDING REMARKS

From the results of an aerodynamic and hydrodynamic investigation to determine the characteristics of the configuration, the following remarks may be made:

The transonic drag rise is abrupt and occurs at a Mach number of about 0.94. The minimum drag coefficient remained nearly constant in the supersonic speed range and is approximately 1.7 times the subsonic minimum drag level. The maximum lift-drag ratio for the configuration with natural transition is approximately 8 at a Mach number of 0.93 and decreases at supersonic speeds to approximately a value of 4 at a Mach number of 2.0.

No appreciable destabilizing tendencies in the longitudinal stability characteristics are encountered through the test lift and Mach number ranges. The maximum variation of the longitudinal stability over the speed range corresponds to a movement of the aerodynamic-center location of about 17 percent of the mean aerodynamic chord.

A stable variation in the lateral and directional stability parameters was obtained throughout the supersonic speed range.

Although this configuration had low aerodynamic damping, the oscillations in trim and rise during take-off and landing were not divergent and the longitudinal stability of the model was satisfactory. Excess

thrust was available for acceleration to take-off. Inlets were free from spray for all gross loads investigated and overloading was limited by the bow clearance.

Langley Aeronautical Laboratory,
    National Advisory Committee for Aeronautics,
        Langley Field, Va., June 19, 1957.

REFERENCES

1. Olson, Roland E., and Bielat, Ralph P.: An Aerodynamic and Hydrodynamic
   Investigation of Two Multijet Water-Based Aircraft Having Low Tran-
   sonic Drag Rise. NACA RM L55A11a, 1955.

2. McKann, Robert E., and Coffee, Claude W.: Limited Hydrodynamic Inves-
   tigation of a 1/15-Size Model of a Modified Nose-Inlet Multijet
   Water-Based Aircraft. NACA RM L55J19, 1956.

3. Bielat, Ralph P., Coffee, Claude W., Jr., and Petynia, William W.:
   Aerodynamic and Hydrodynamic Characteristics of a Deck-Inlet Multi-
   jet Water-Based-Aircraft Configuration Designed for Supersonic
   Flight. NACA RM L56H01, 1956.

4. Morse, Archibald E., Jr., Woodward, David R., and Blanchard, Ulysse J.:
   An Investigation of the Hydrodynamic Characteristics of a Dynamic
   Model of a Transonic Seaplane Design Having a Planing-Tail Hull.
   NACA RM L56C28a, 1956.

5. Blanchard, Ulysse J.: Hydrodynamic Investigation of a Model of a
   Supersonic Multijet Water-Based Aircraft With Engines Exhausting
   From the Step. NACA RM L57F20, 1957.

6. Gorton, Gerald C.: Investigation at Supersonic Speeds of a Translating-
   Spike Inlet Employing a Steep-Lip Cowl. NACA RM E54G29, 1954.

7. Carmel, Melvin M., and Fischetti, Thomas L.: A Transonic Wind-Tunnel
   Investigation of the Effects of Nacelles on the Aerodynamic Charac-
   teristics of a Complete Model Configuration. NACA RM L53F22a, 1953.

8. Goodson, Kenneth W.: Static Longitudinal Characteristics at High Sub-
   sonic Speeds of a Complete Airplane Model With a Highly Tapered Wing
   Having the 0.80 Chord Line Unswept and With Several Tail Configura-
   tions. NACA RM L56J03, 1956.

9. Campbell, John P., and Johnson, Joseph L., Jr.: Wind-Tunnel Investi-
   gation of an External-Flow Jet-Augmented Slotted Flap Suitable for
   Application to Airplanes With Pod-Mounted Jet Engines. NACA TN 3898,
   1956.

10. Schnitzer, Emanuel: Reduction of Hydrodynamic Impact Loads for Water-
   borne Aircraft. NACA RM L55E09b, 1955.

11. Weinstein, Irving, and Kapryan, Walter J.: The High-Speed Planing
   Characteristics of a Rectangular Flat Plate Over a Wide Range of
   Trim and Wetted Length. NACA TN 2981, 1953.

12. Hoffman, Sherwood, Wolff, Austin L., and Faget, Maxime A.: Flight
    Investigation of the Supersonic Area Rule for a Straight Wing-
    Body Configuration at Mach Numbers Between 0.8 and 1.5. NACA
    RM L55C09, 1955.

13. Whitcomb, Richard T.: Some Considerations Regarding the Application
    of the Supersonic Area Rule to the Design of Airplane Fuselages.
    NACA RM L56E23a, 1956.

14. Truscott, Starr: The Enlarged N.A.C.A. Tank, and Some of Its Work.
    NACA TM 918, 1939.

15. Olson, Roland E., and Land, Norman S.: Methods Used in the NACA
    Tank for the Investigation of the Longitudinal-Stability Character-
    istics of Models of Flying Boats. NACA Rep. 753, 1943. (Supersedes
    NACA WR L-409.)

16. Spearman, M. Leroy: Investigation of the Aerodynamic Characteristics
    in Pitch and Sideslip of a 45° Sweptback-Wing Airplane Model With
    Various Vertical Locations of the Wing and Horizontal Tail - Effect
    of Wing Location and Geometric Dihedral for the Wing-Body Combina-
    tion, M = 2.01. NACA RM L55B18, 1955.

TABLE I.- PERTINENT CHARACTERISTICS AND DIMENSIONS OF THE FULL-SIZE WATER-BASED AIRCRAFT

General:
Gross weight, lb 225,000
Wing area, sq ft 1,500
Engines, advanced Orenda Iroquois PS-13 with afterburners 4
Take-off thrust (with afterburners), lb 126,000
Take-off wing loading, lb/sq ft 150
Take-off thrust-weight ratio 0.56
Total surface area, sq ft 9,549

Wing:
Span, ft 72.5
Wing area, sq ft 1,500
Airfoil section . . . . NACA 65A003
Aspect ratio 3.5
Taper ratio 0.067
Sweepback $(0.25\bar{c})$, deg 28.9
Sweepback $(0.80\bar{c})$, deg 0
Dihedral, deg 0
Length, mean aerodynamic chord, ft 26.0
Incidence, deg . . . . $2\frac{1}{2}$ to 10
Twist, deg 0

Horizontal tail:
Span, ft 30.3
Airfoil section . . . . NACA 65A004
Area, sq ft 230
Aspect ratio 4.0
Taper ratio 0
Sweepback $(0.25\bar{c})$, deg 36.9
Dihedral, deg 0
Arm, between $\bar{c}/4$ of wing to $\bar{c}/4$ of horizontal tail, ft 52.0

Vertical tail:
Airfoil . . . . NACA 65A006
Aspect ratio 1.2
Sweepback $(0.25\bar{c})$, deg 41.2

Fuselage:
Length, overall, ft 158.3
Width, maximum, ft 7.9
Height, maximum, ft 13.0
Afterbody dead rise, deg 20
Sternpost angle, deg 1.8
Center of gravity, above fuselage base line, ft 6.9
Fuselage volume, cu ft 7,161
Ratio of normal gross load to total fuselage displacement 0.49

Hydro-ski:
Maximum length, ft 38.7
Maximum beam, ft 6.7
Length-beam ratio 5.8
Area, sq ft 215.5
Beam-loading coefficient, C_{Δ_0} 11.9
$\dfrac{\text{Gross weight}}{\text{Ski area}}$, lb/sq ft 1,044
Incidence, deg 2.0
Distance of trailing edge below fuselage base line, ft 11.8
Distance of trailing edge ahead of $\bar{c}/4$, ft 0.6
Sternpost angle, deg 10.0

Area curve:
Maximum net cross-sectional area, sq ft 107
Maximum diameter of equivalent body, ft 11.7
Length, ft 158.3
Fineness ratio of equivalent body 13.6

Figure 1.- General arrangement of configuration.
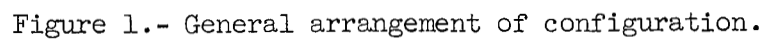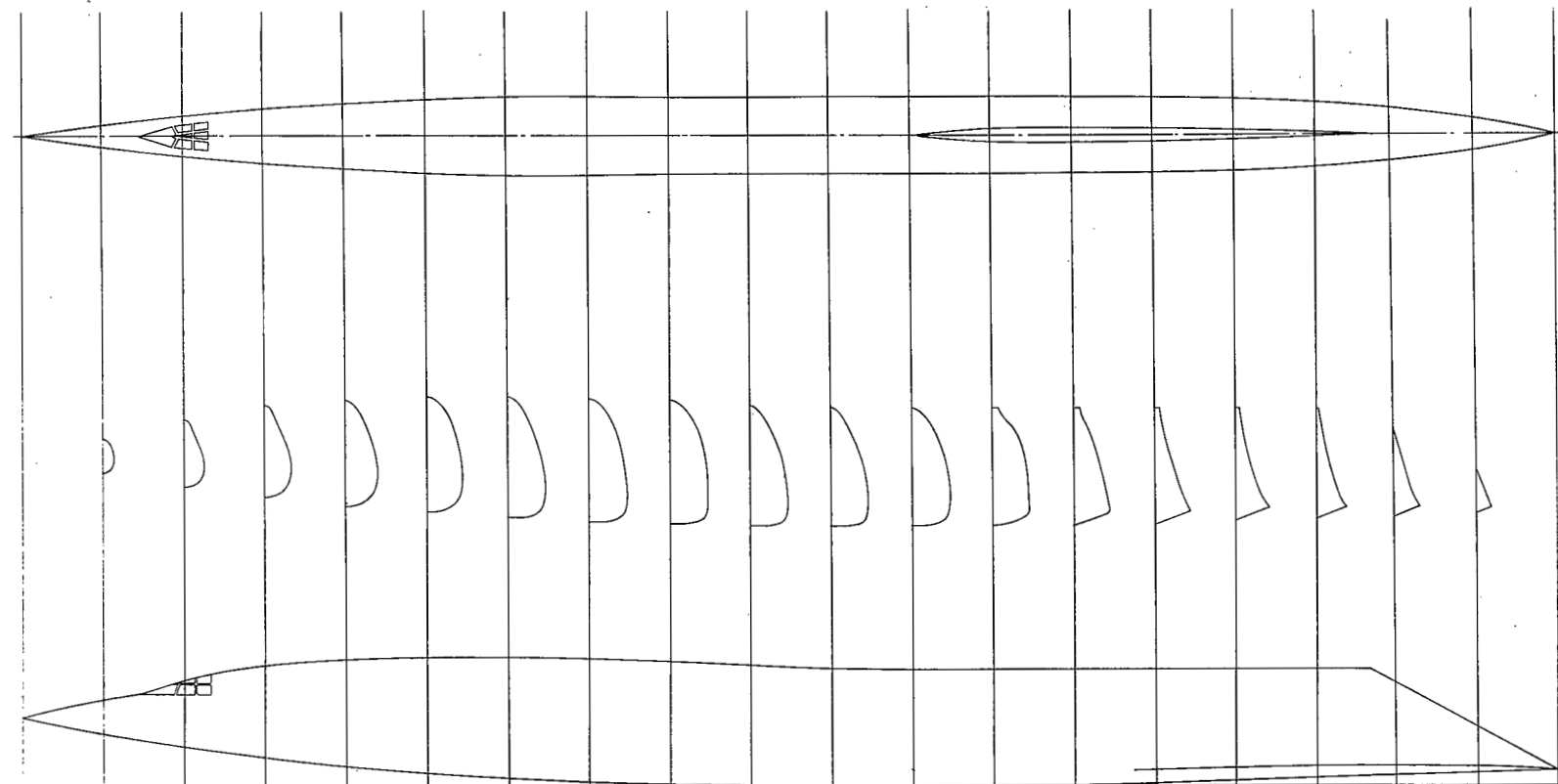
Figure 2.- Layout of fuselage lines.
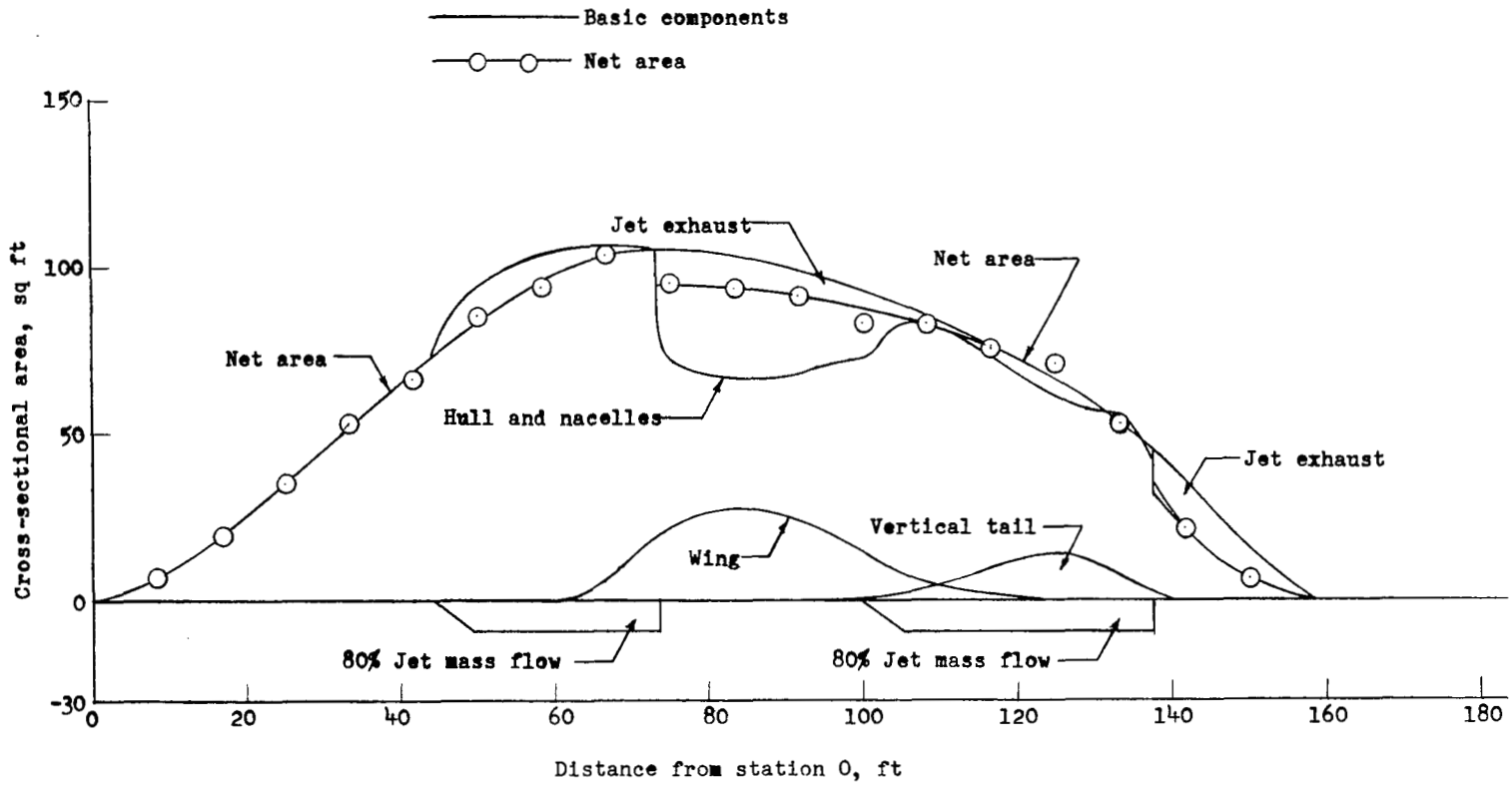
Figure 3.- Cross-sectional-area curves. M = 1.4.

Side force

Yawing moment

Relative wind

β

A

A

A

Lift force

Pitching moment

α

$-i_t$

Rolling moment

Relative wind

Drag force

View A-A
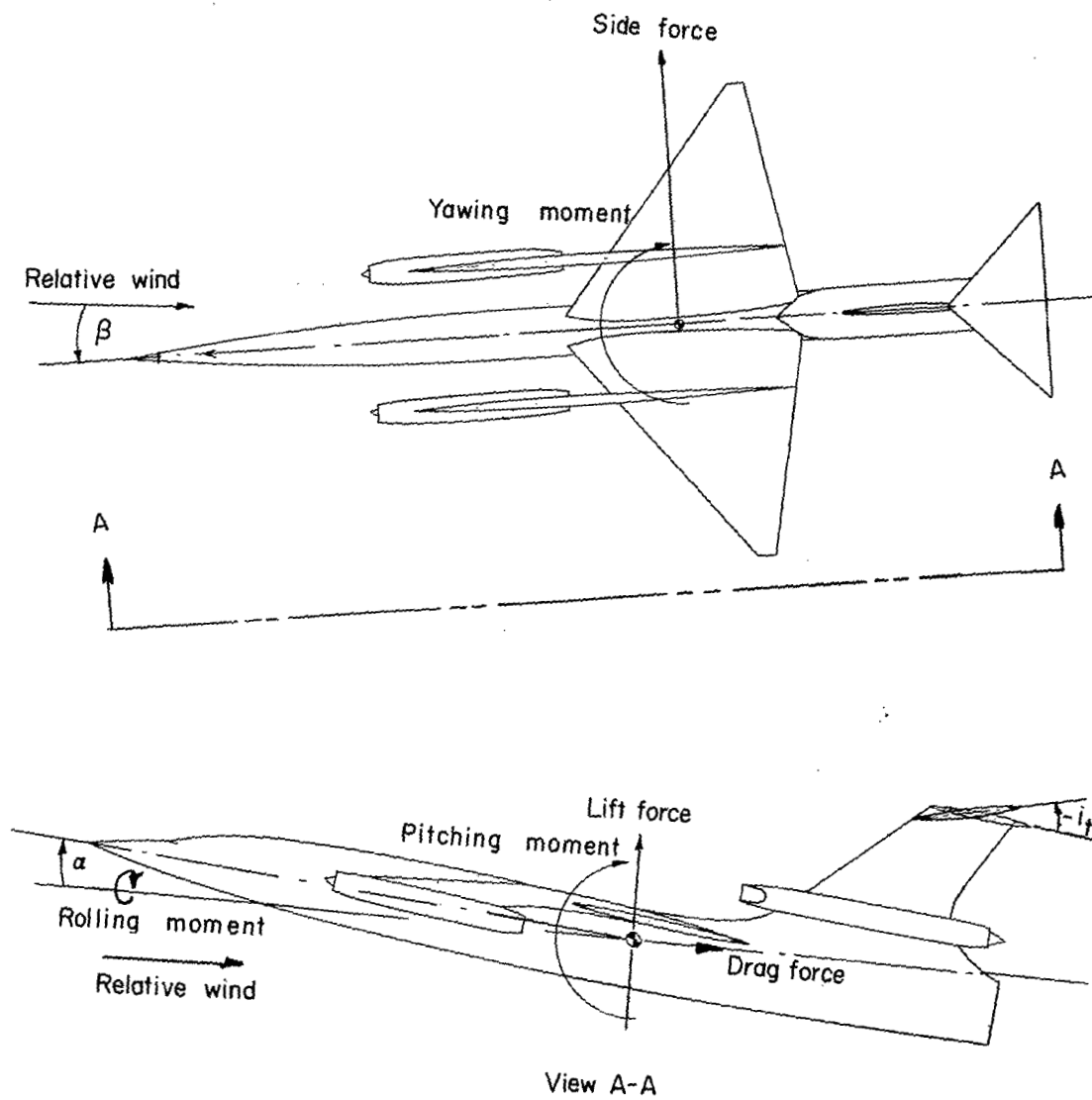
Figure 4.- Stability-axes system.
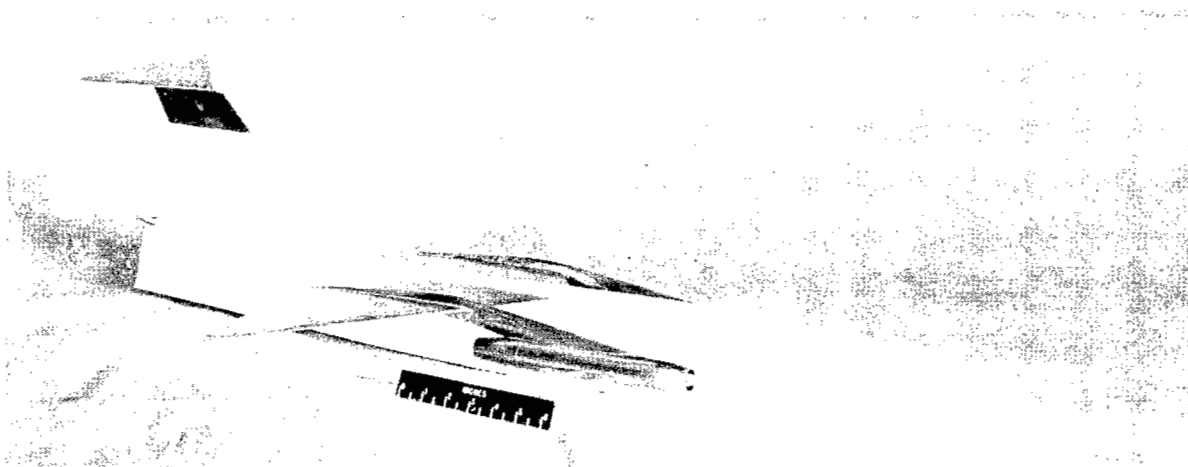
L-93342
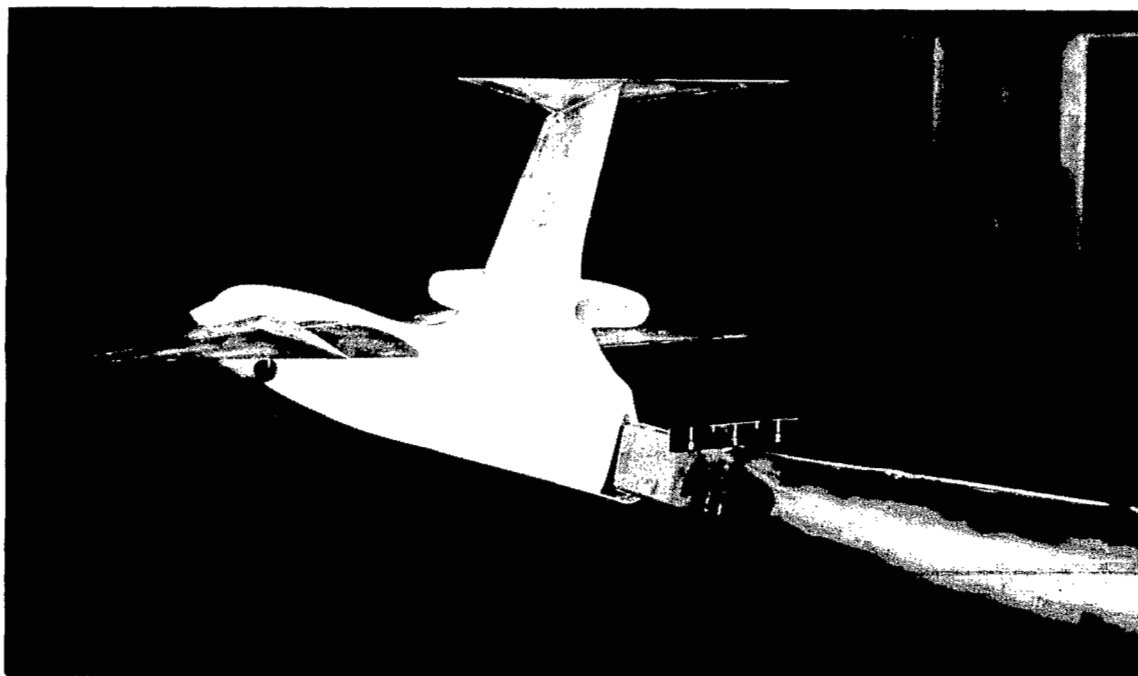
Figure 5.- Photographs of 1/42.5-scale wind-tunnel model.   L-94578
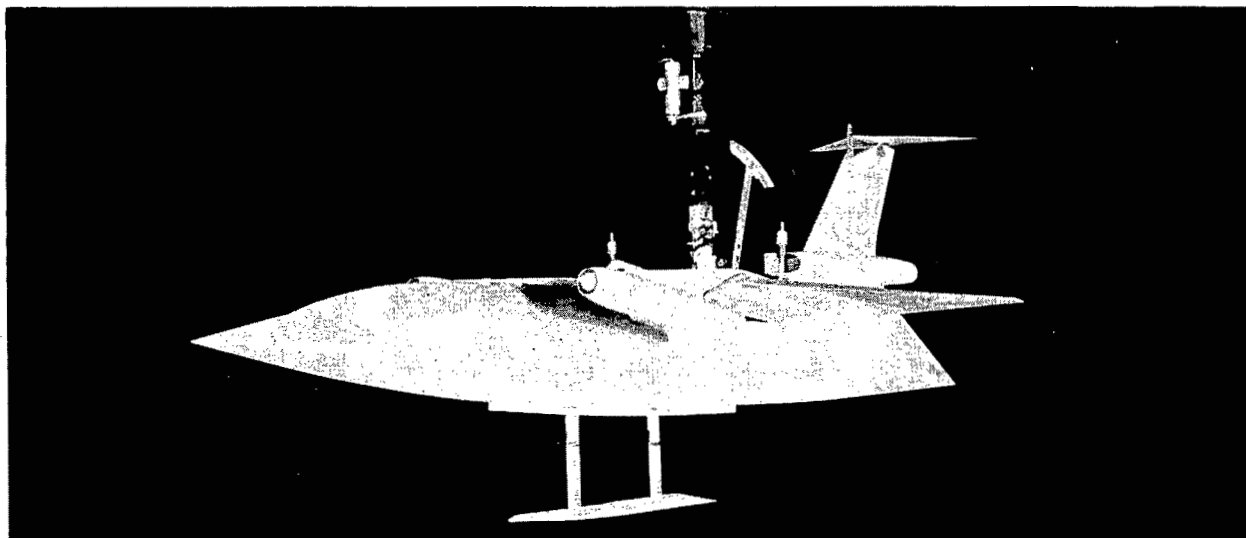
L-94468
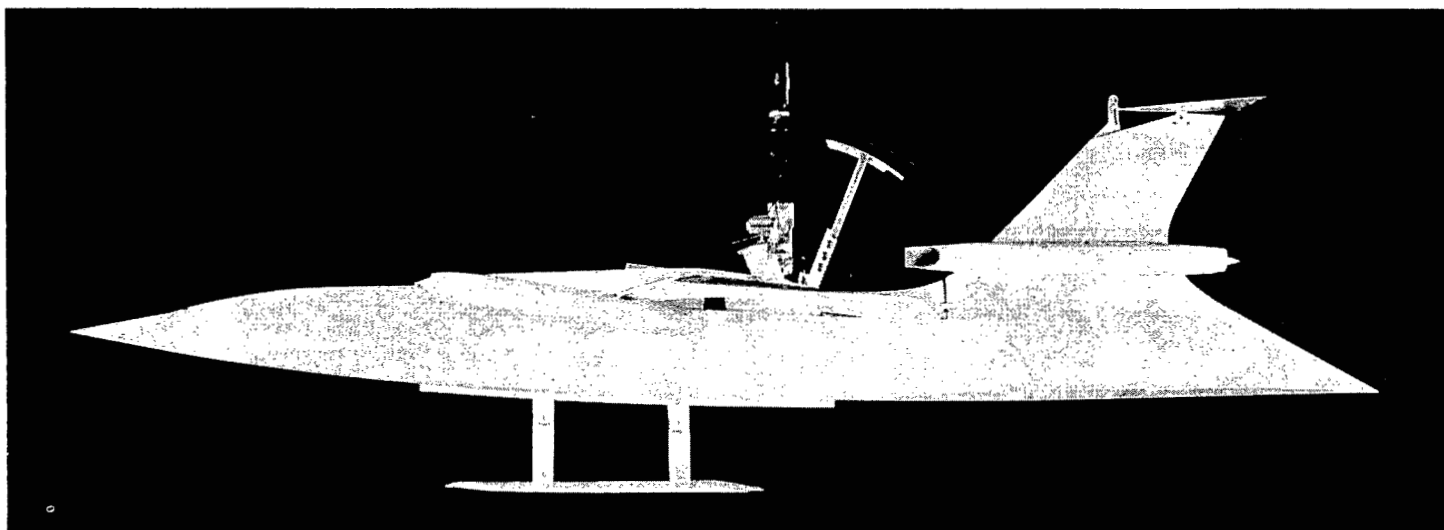
L-94467

Figure 6.- Photographs of 1/20-size tank model.
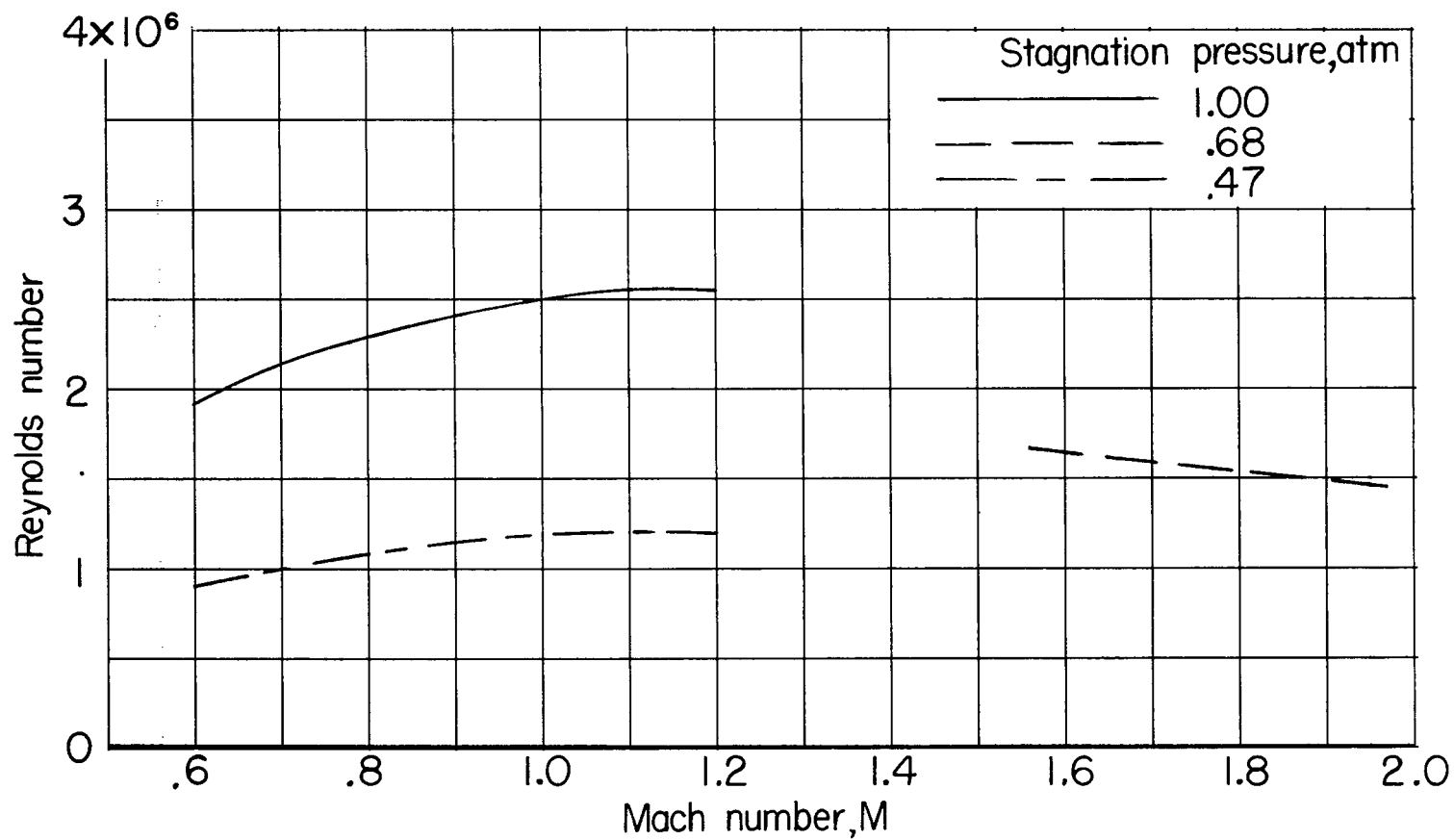
Figure 7.- Variation of Reynolds number based on $\bar{c}$ with Mach number.
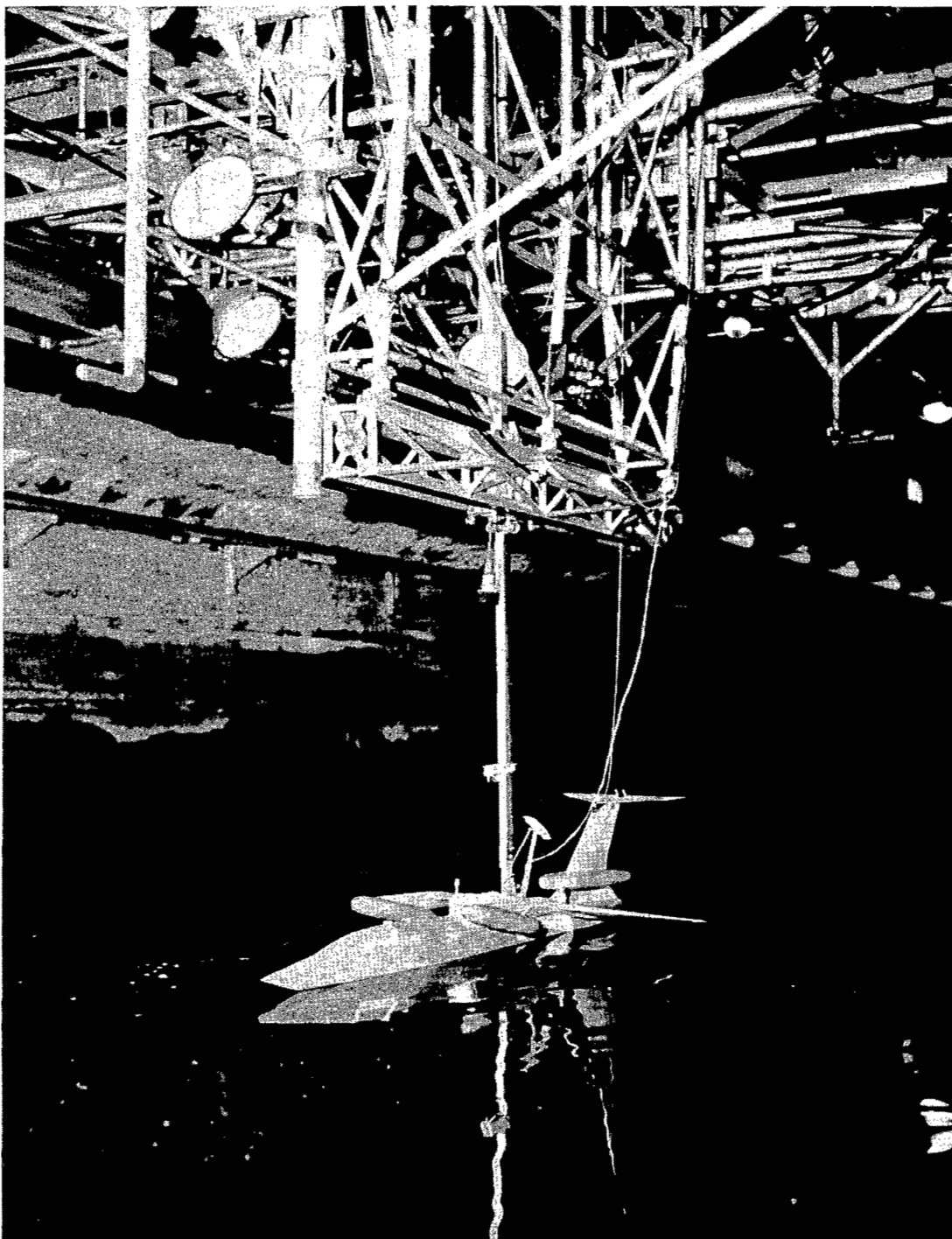
Figure 8.- Setup of model on towing gear.   L-57-1631
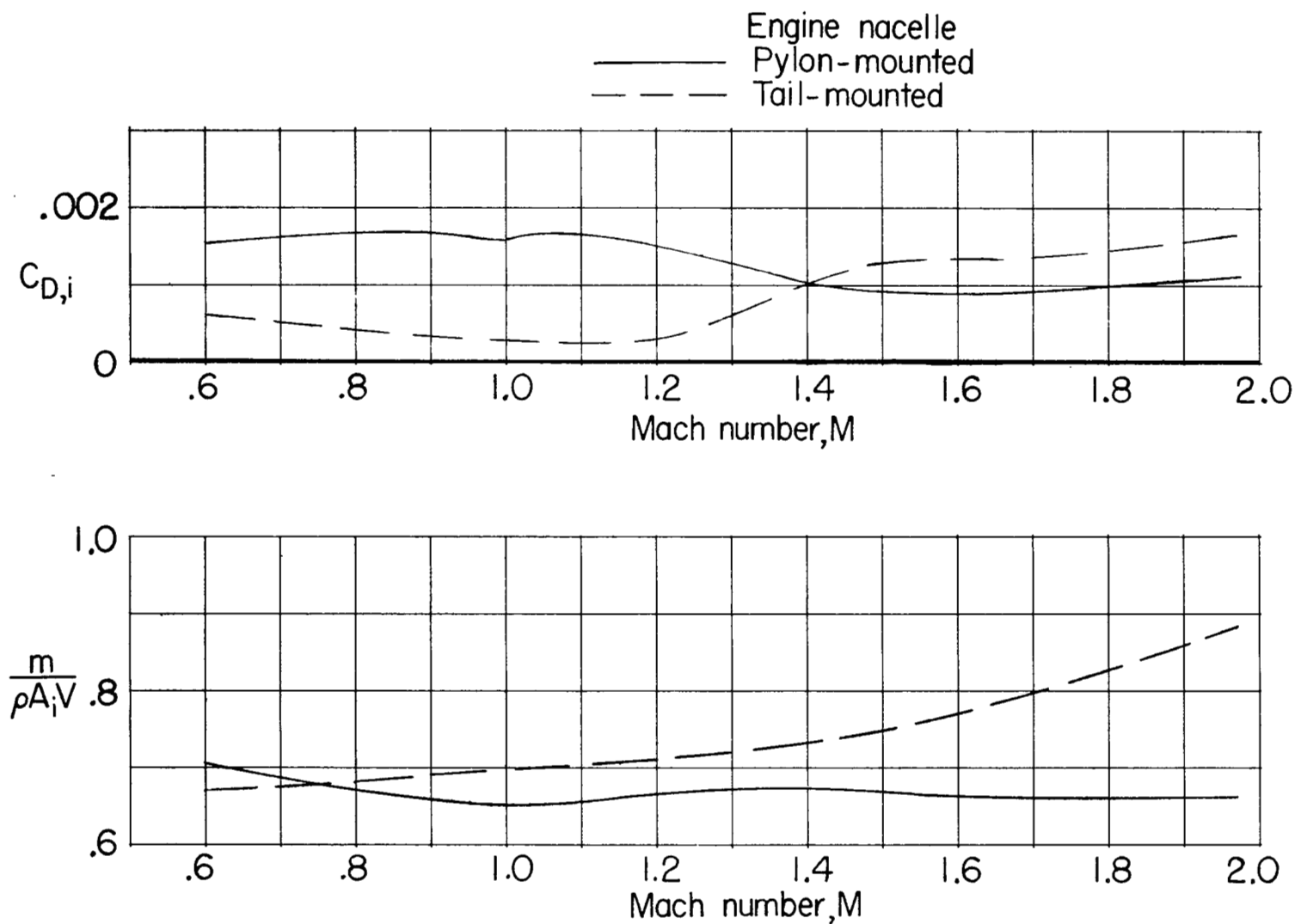
Figure 9.- Variation of nacelle internal-drag coefficient and inlet mass-flow ratio with Mach number. $\alpha = 0°$.
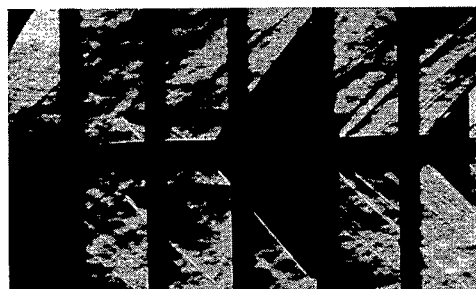
$\phi=0°; \alpha\approx0°$ M=1.56 $\phi=90°; \alpha\approx2.5°$
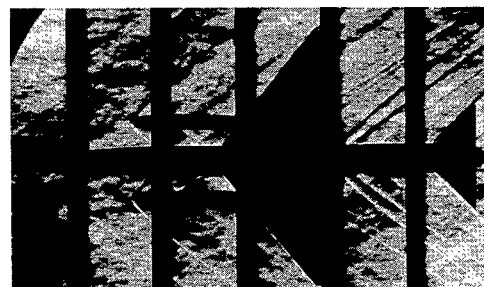
$\phi=0°; \alpha\approx0°$ M=1.77 $\phi=90°; \alpha\approx2.5°$
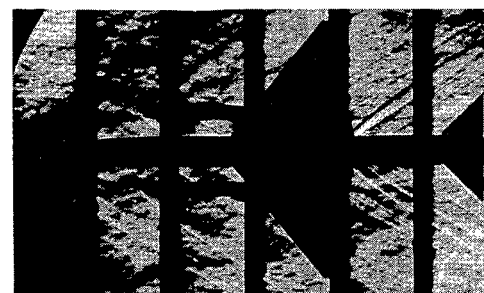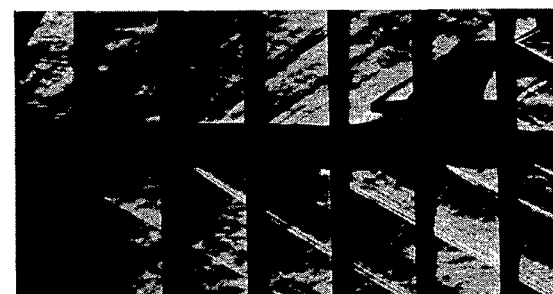
$\phi=0°; \alpha\approx0°$ M=1.97 $\phi=90°; \alpha\approx2.5°$

L-57-1632

Figure 10.- Schlieren photographs of model in Unitary Plan wind tunnel. Natural transition; $i_t = -2.5°$; $\beta \approx 0°$.
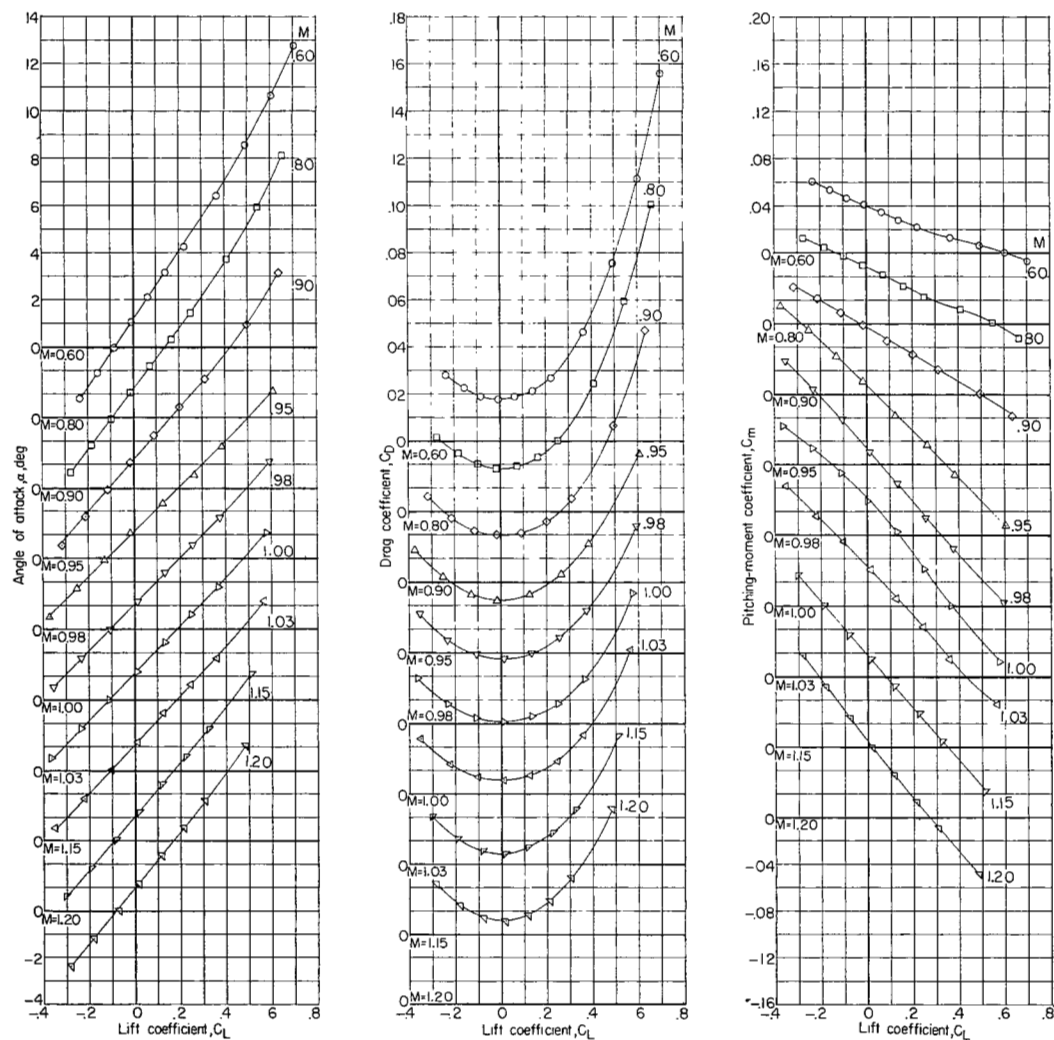
Figure 11.- Aerodynamic characteristics of the model. Natural transition; $i_t = -2.5°$; stagnation pressure, 1 atmosphere.
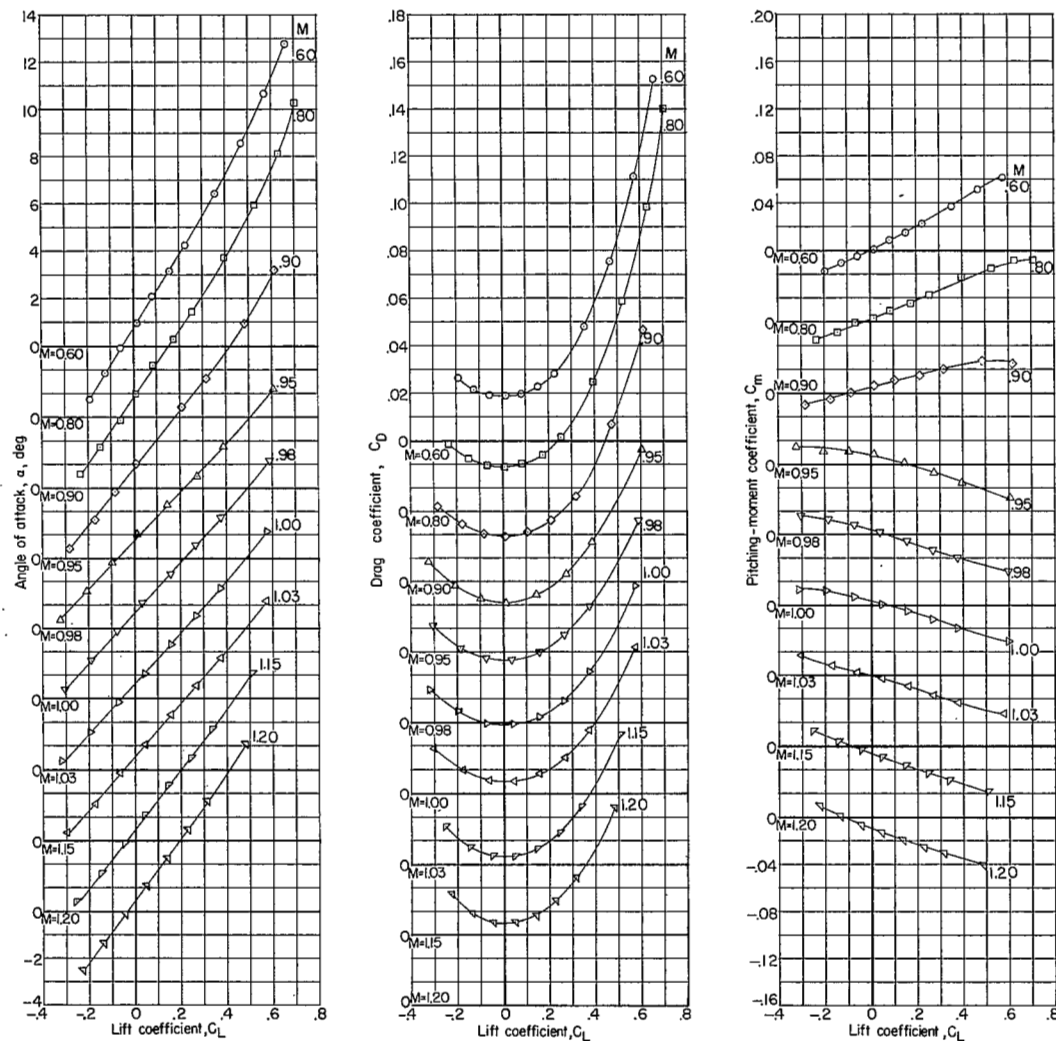
Figure 12.- Aerodynamic characteristics of the model without the horizontal tail. Fixed transition; stagnation pressure, 1 atmosphere.
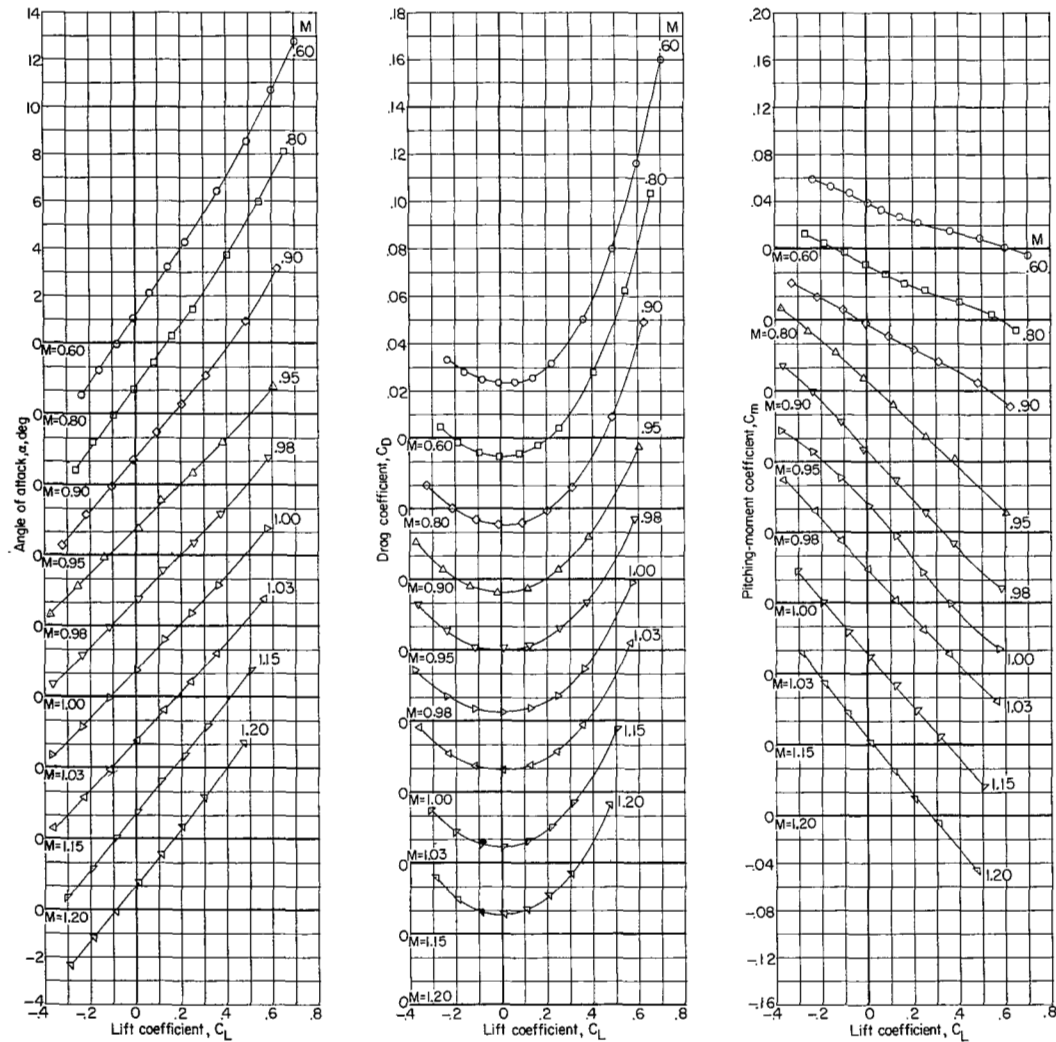
Figure 13.- Aerodynamic characteristics of the model. Fixed transition; i_t = -2.5°; stagnation pressure, 1 atmosphere.
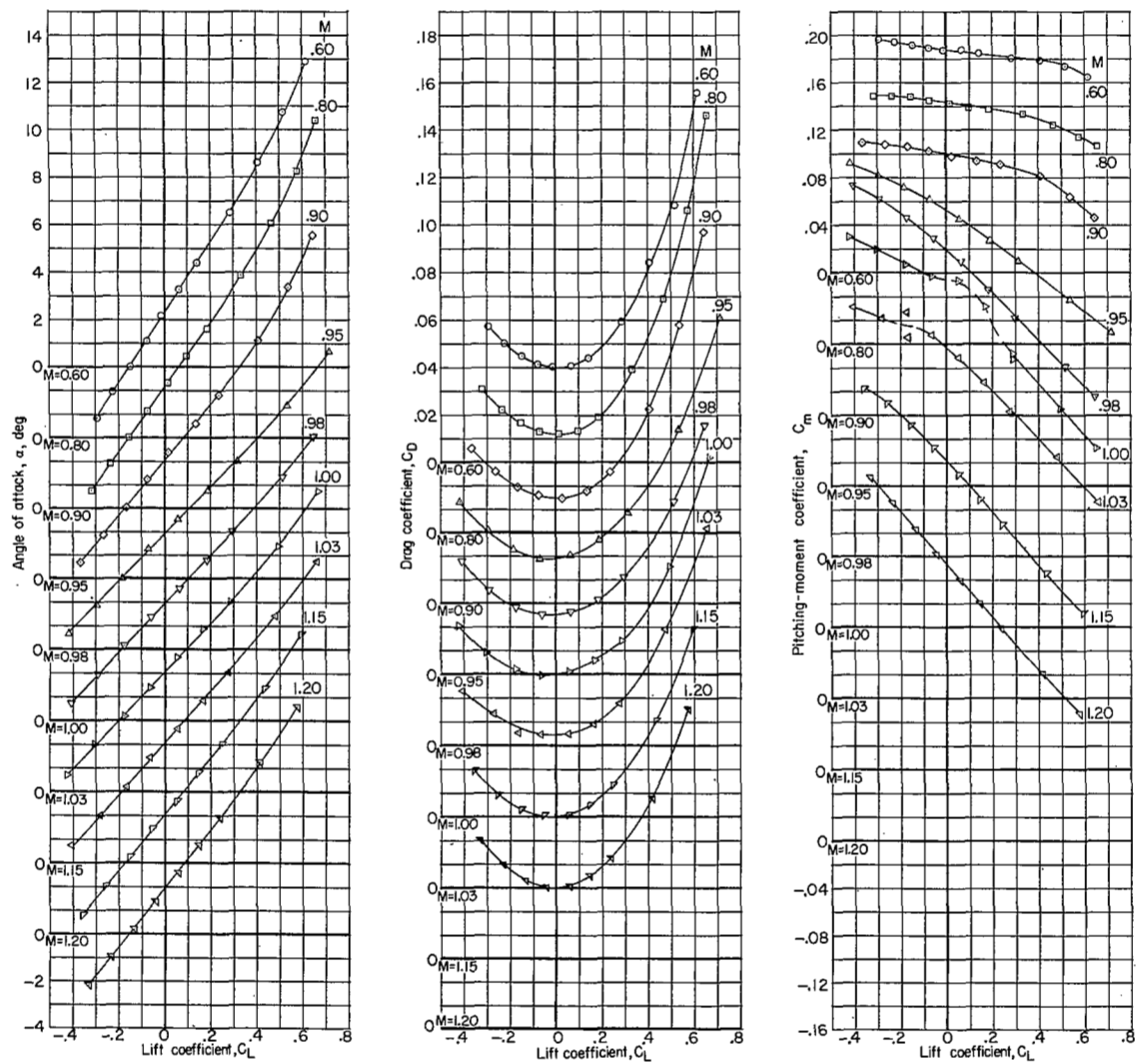
Figure 14.- Aerodynamic characteristics of the model. Fixed transition; i_t = -12.5°; stagnation pressure, 1 atmosphere.
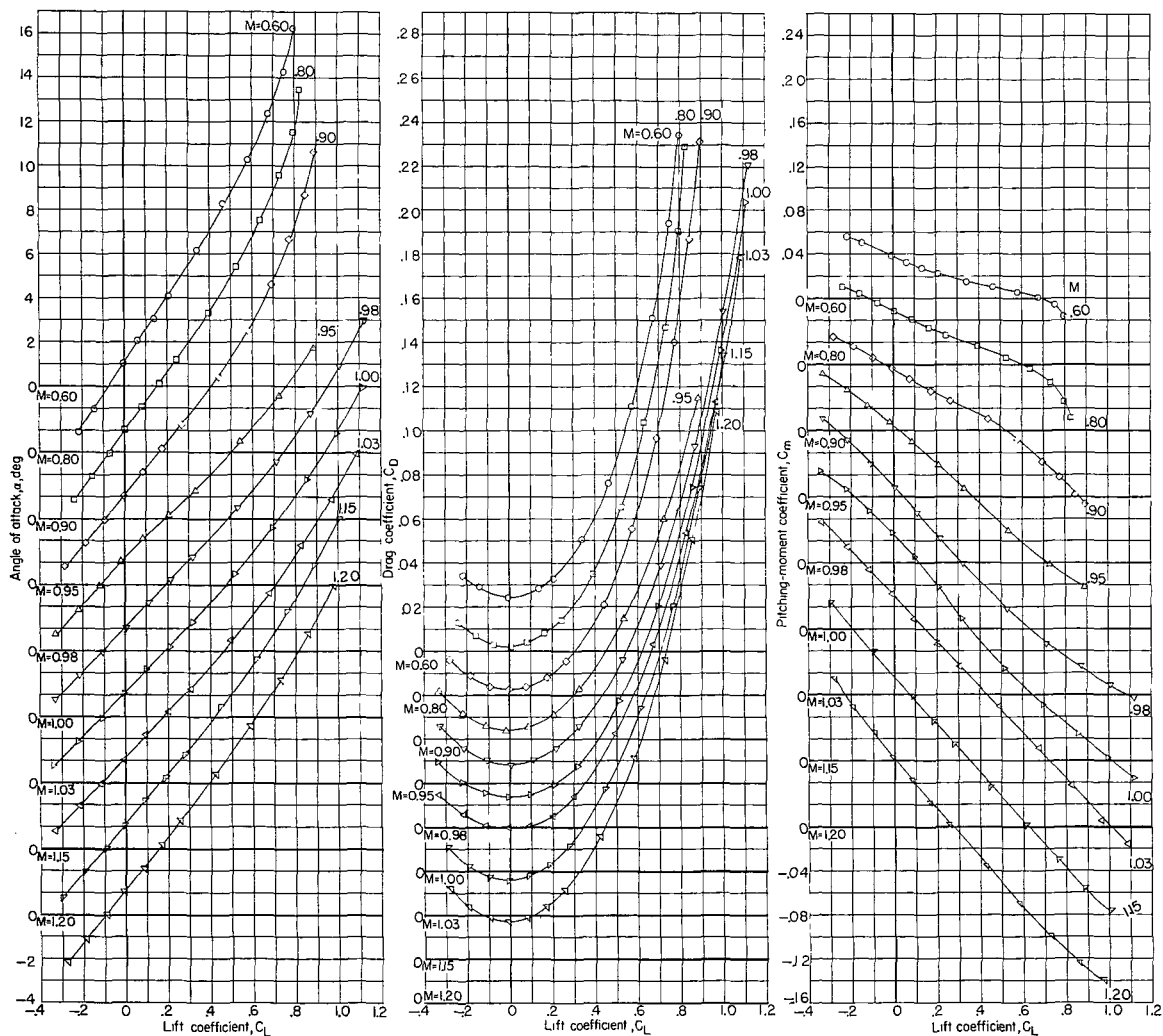
Figure 15.- Aerodynamic characteristics of the model. Fixed transition; i_t = -2.5°; stagnation pressure, 0.47 atmosphere.
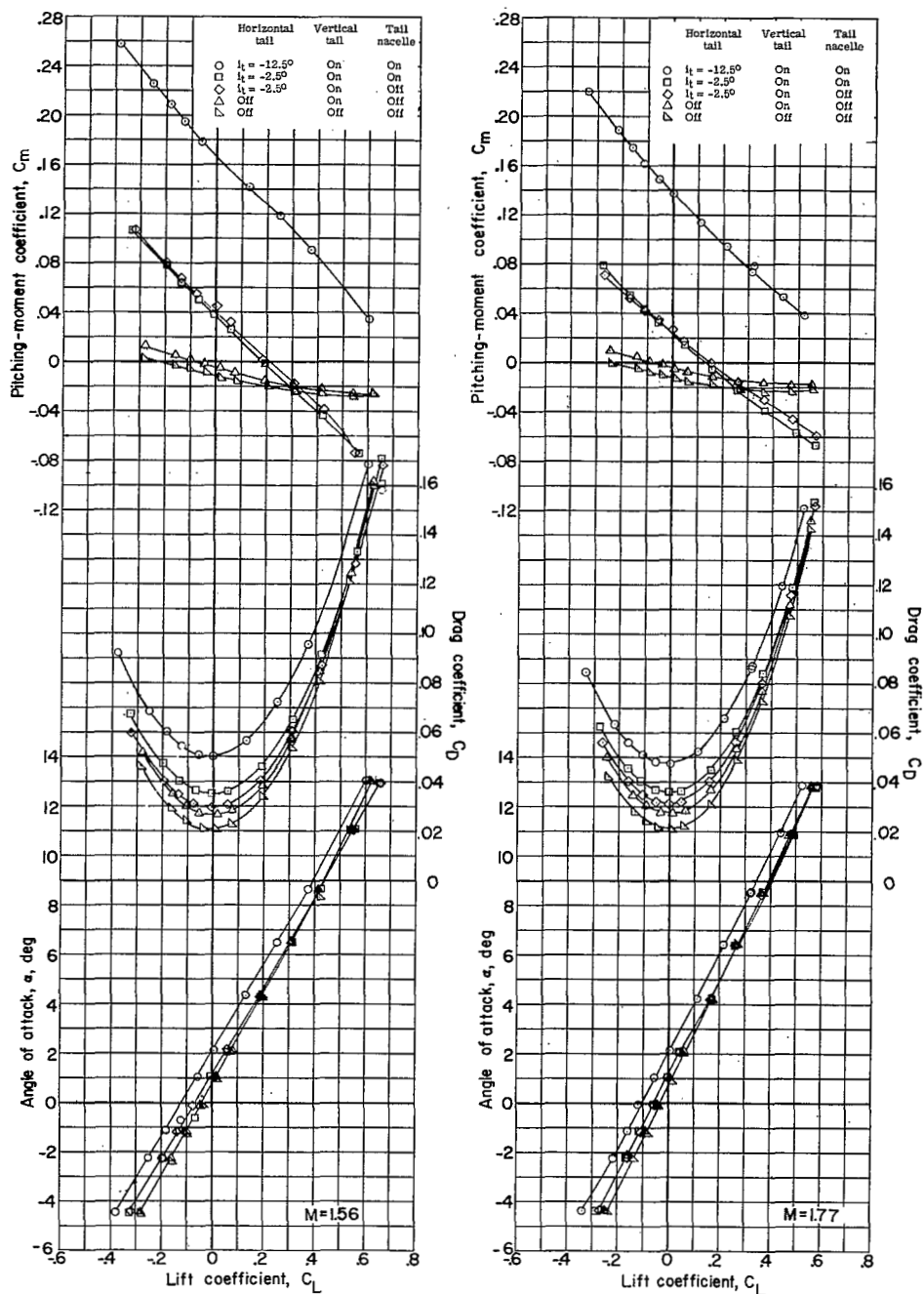
(a) M = 1.56 and M = 1.77.

Figure 16.- Aerodynamic characteristics in pitch of the model.
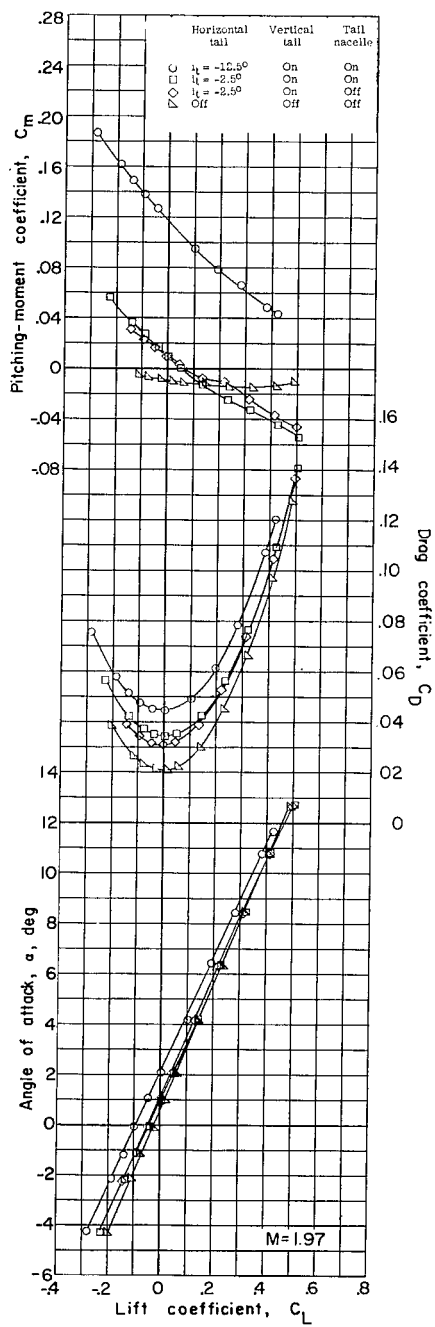
(b) M = 1.97.

Figure 16.- Concluded.
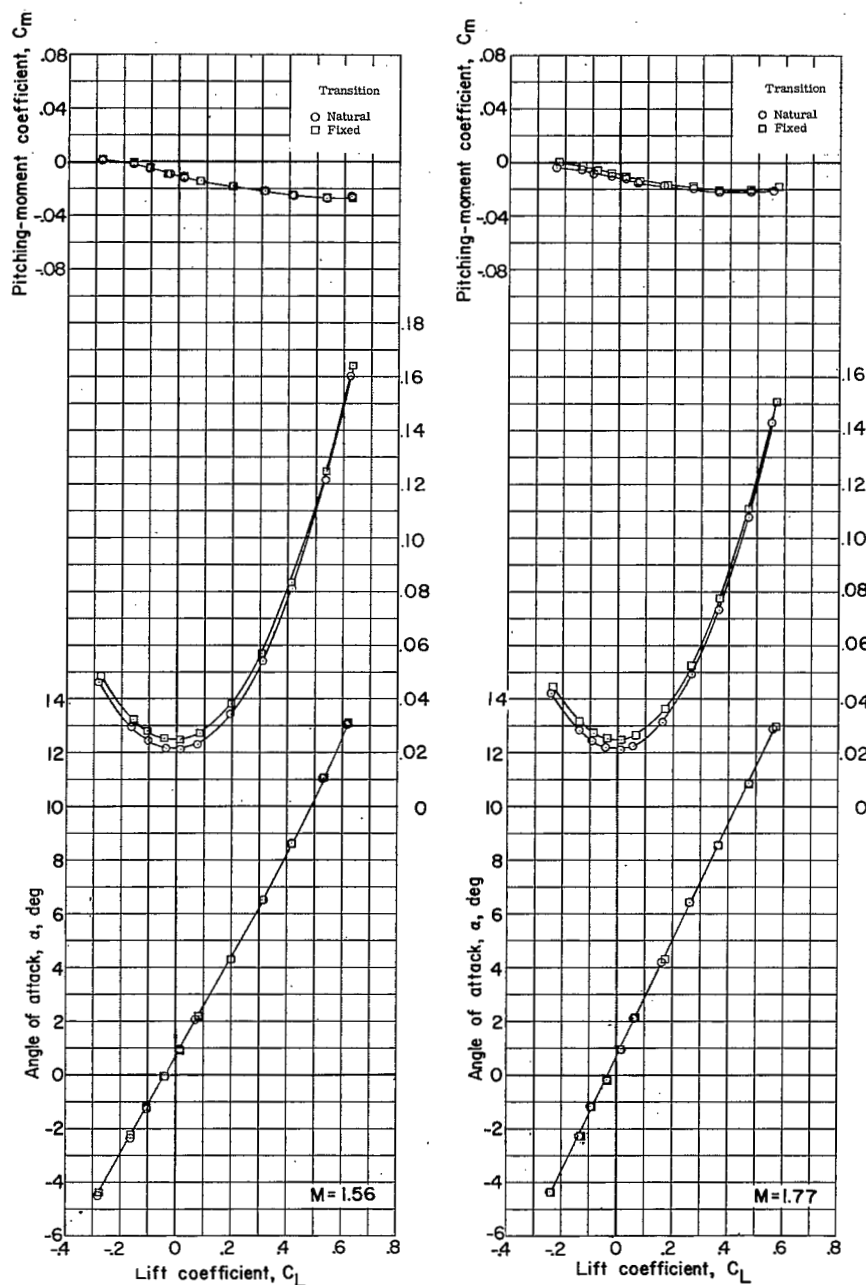
(a)   M = 1.56   and   M = 1.77.

Figure 17.- Summary of the effect of transition on the aerodynamic char-
acteristics in pitch of the wing—fuselage—pylon-mounted-nacelle com-
bination of the model.
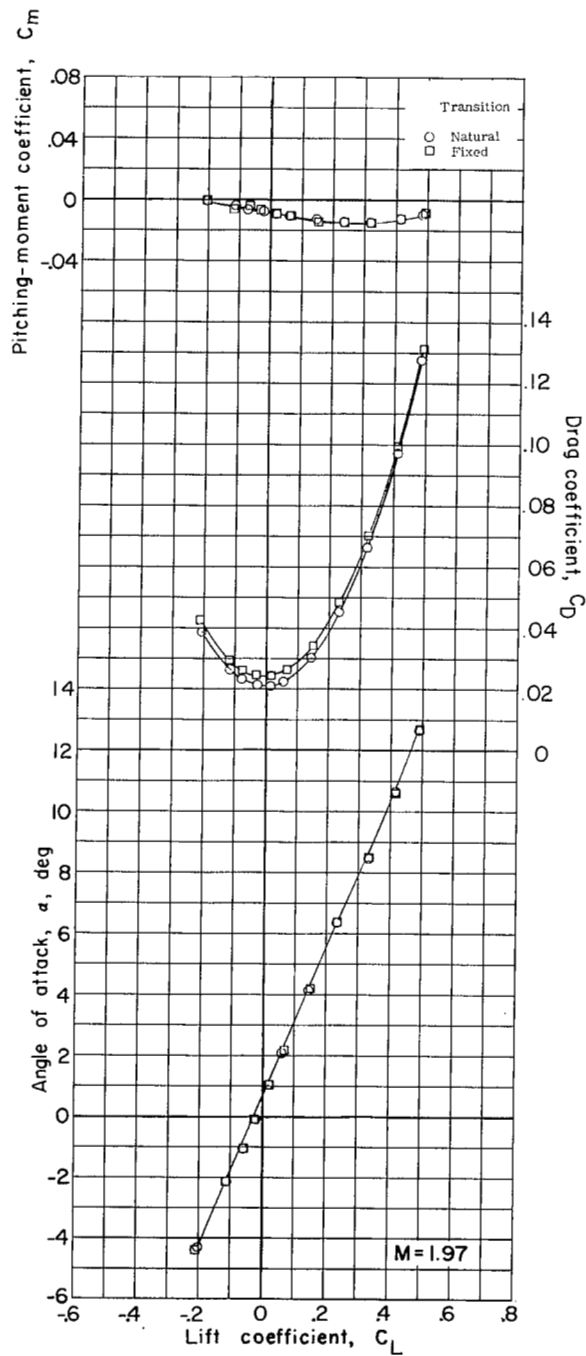
(b)   M = 1.97.

Figure 17.- Concluded.
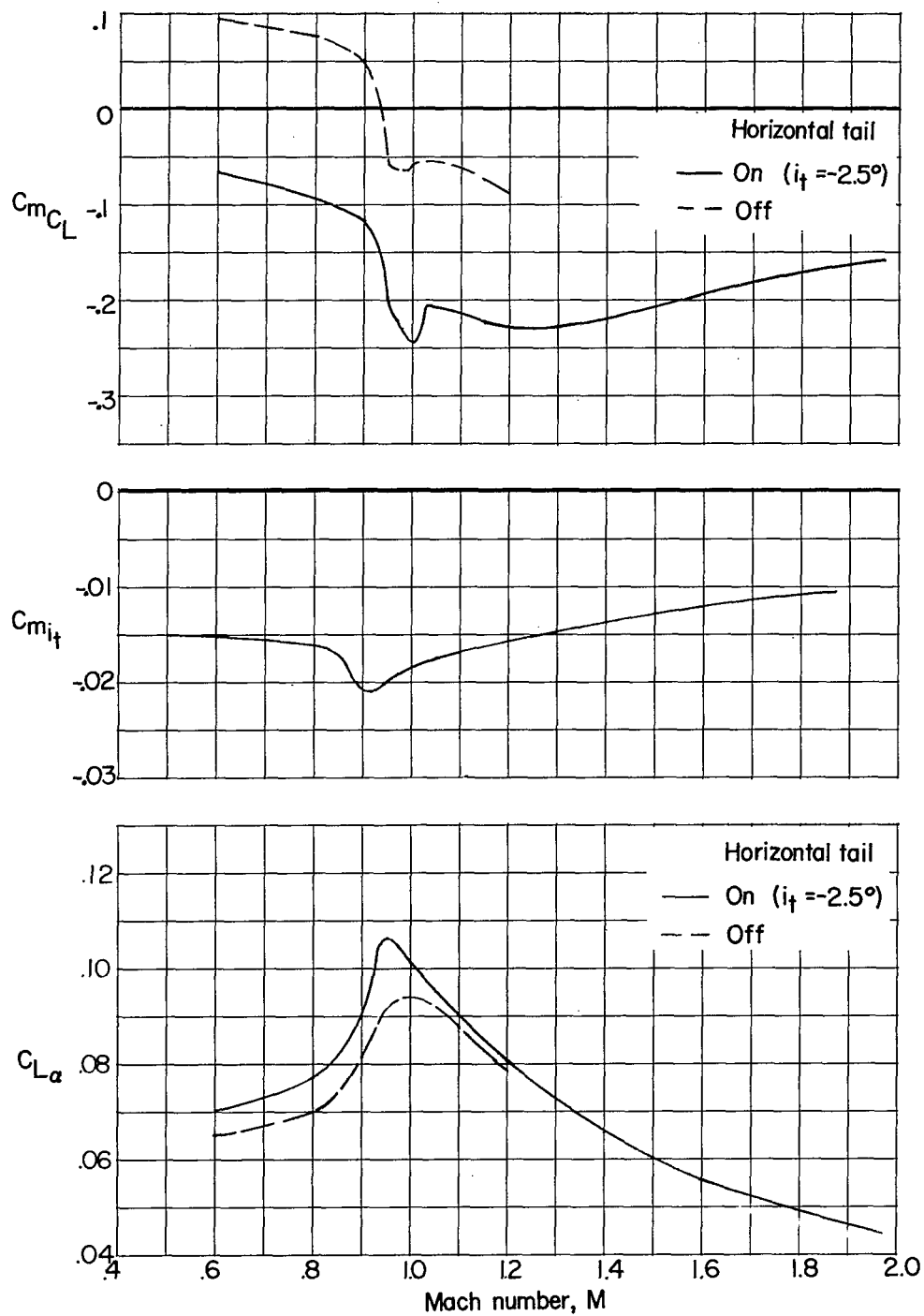
Figure 18.- Summary of aerodynamic characteristics in pitch at transonic and supersonic speeds for the model.
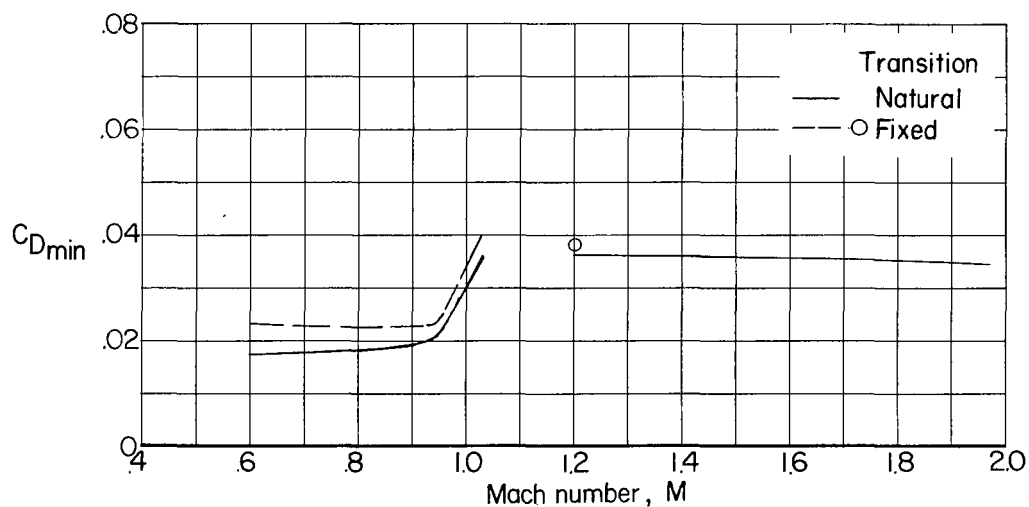
Figure 19.- Variation of minimum drag coefficient $C_{D_{min}}$ with Mach number for the model. $i_t = -2.5^o$.
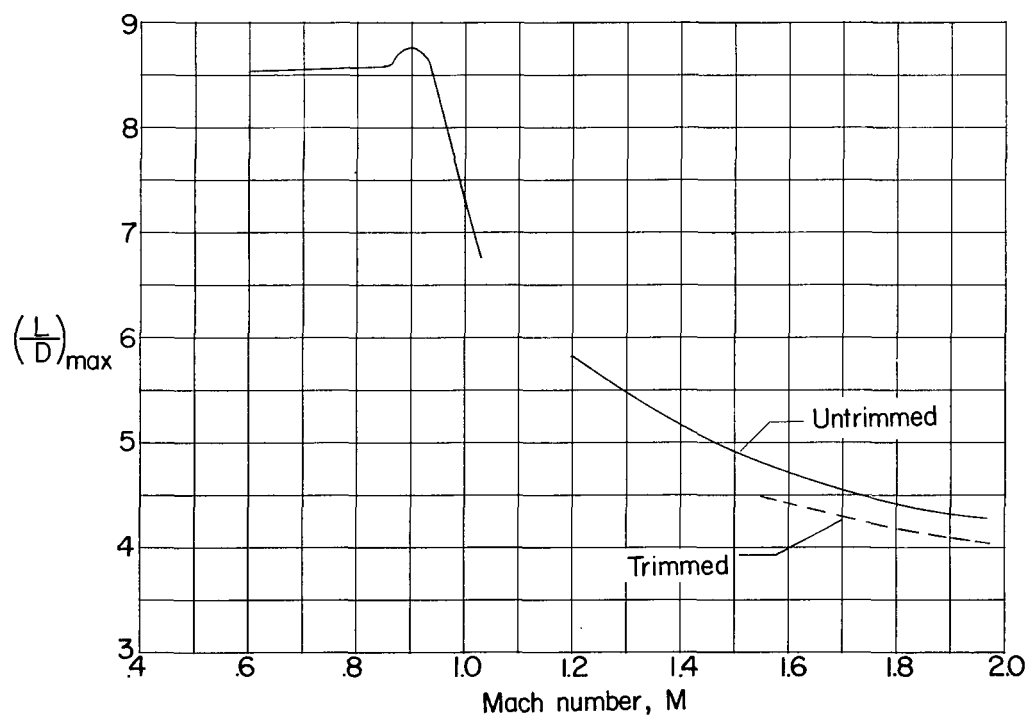
Figure 20.- Variation of maximum lift-drag ratio $(L/D)_{max}$ with Mach number for the model. $i_t = -2.5^o$; natural transition.
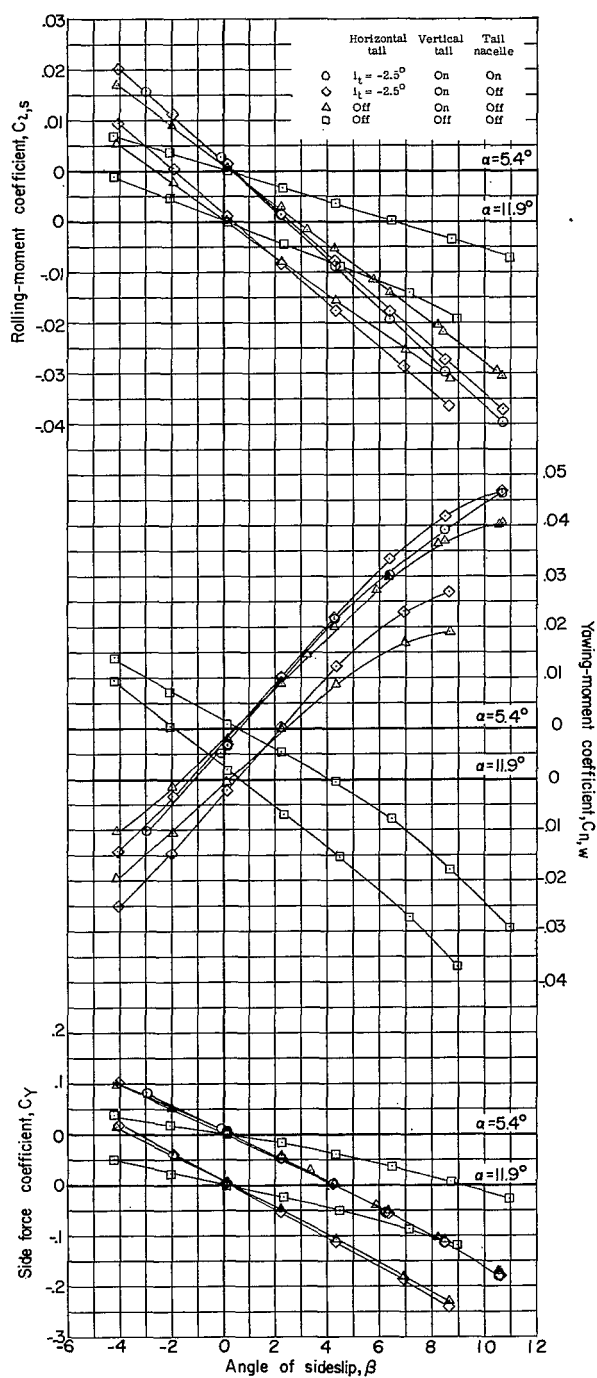
(a)   M = 1.56.

Figure 21.- Aerodynamic characteristics in sideslip of the model.
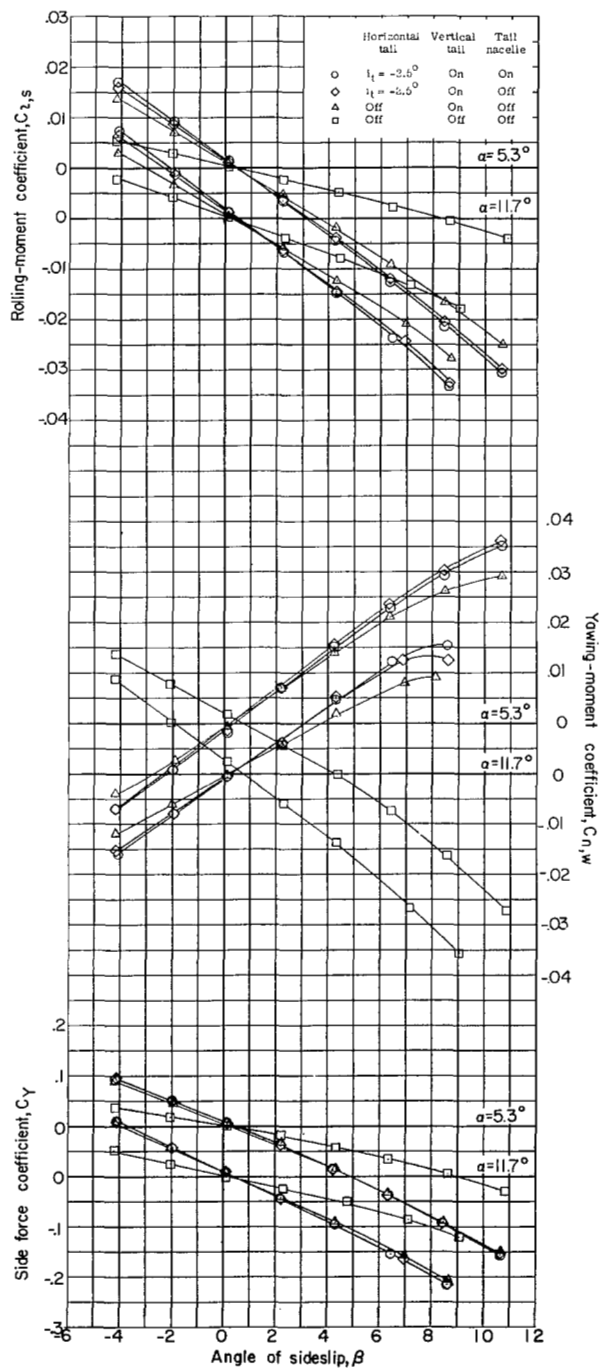
(b)   M = 1.77.

Figure 21.- Continued.
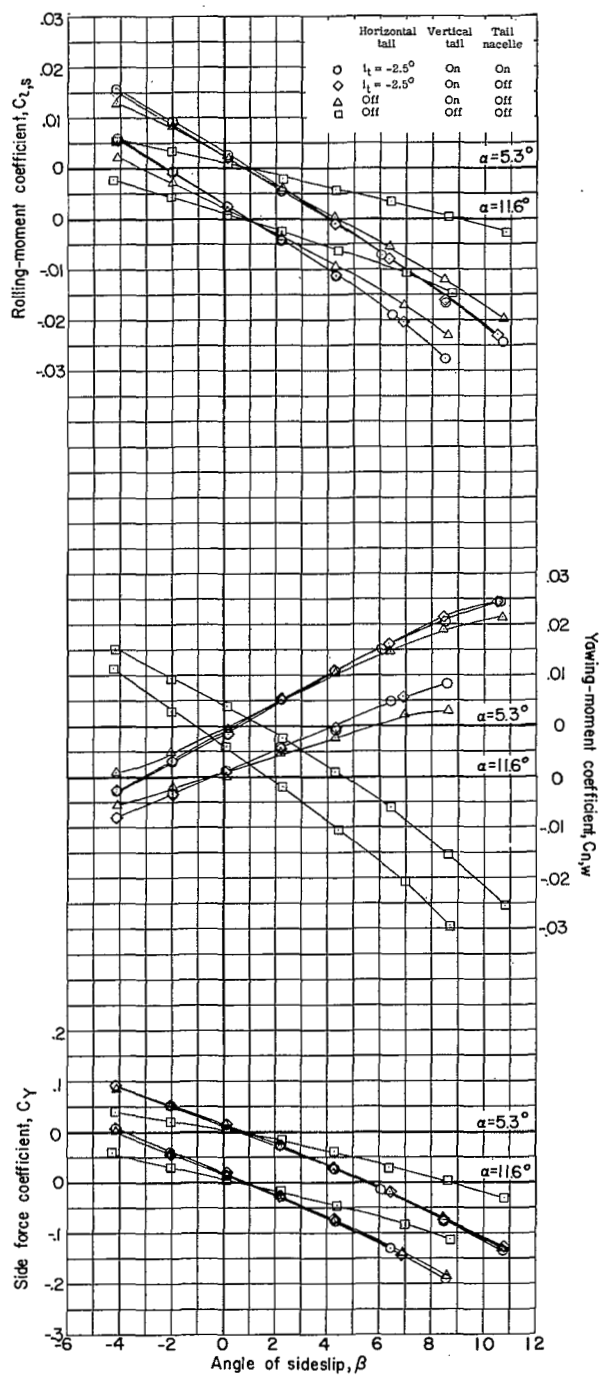
(c)   M = 1.97.

Figure 21.- Concluded.
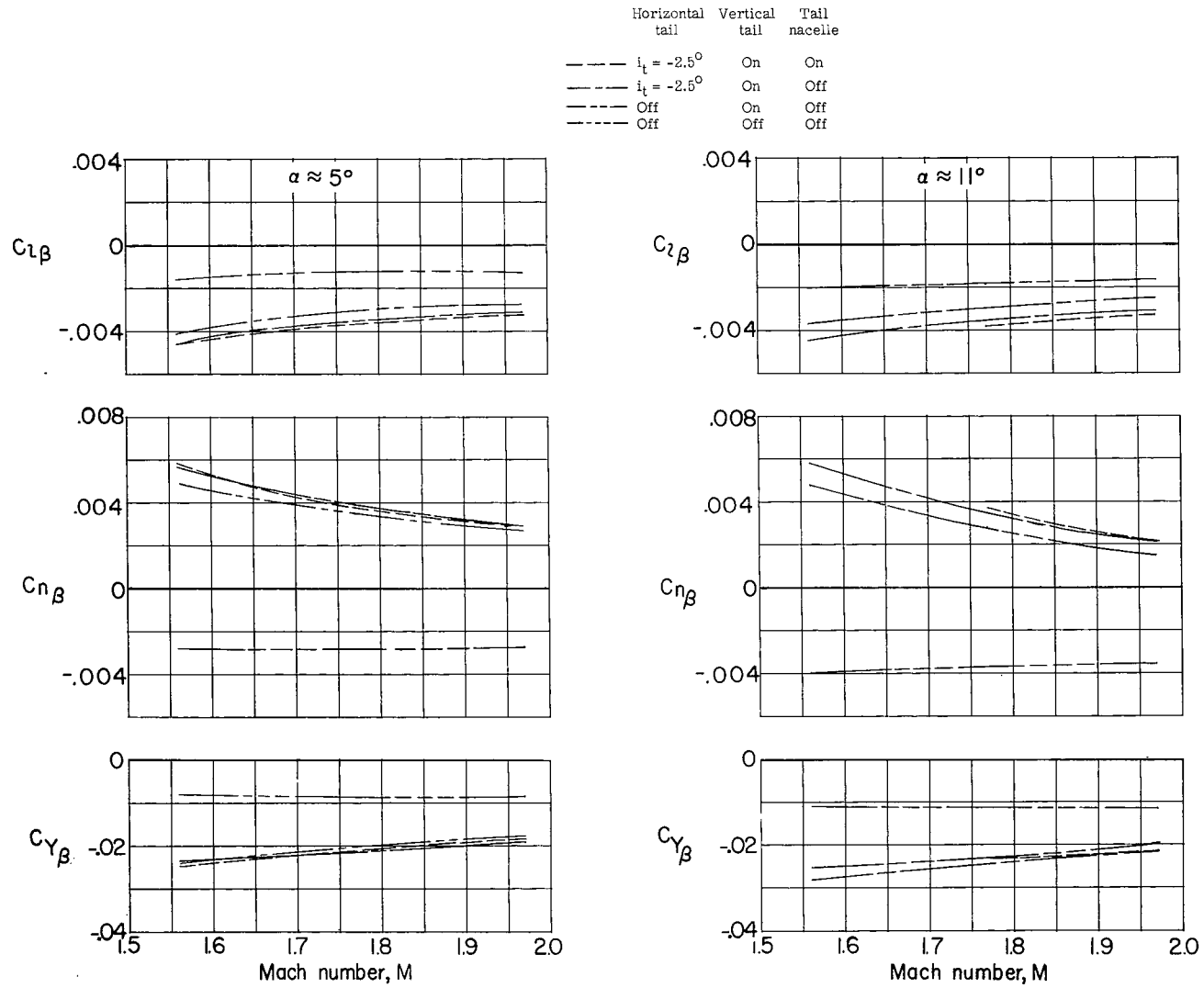
Figure 22.- Summary of the lateral stability parameters of the model.
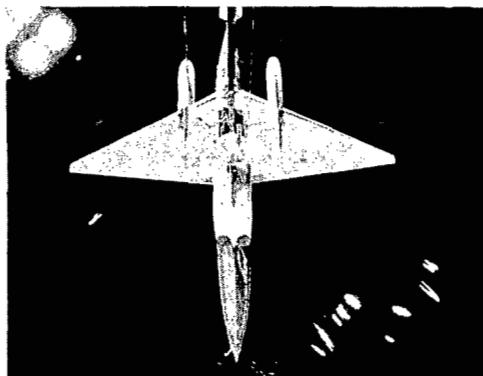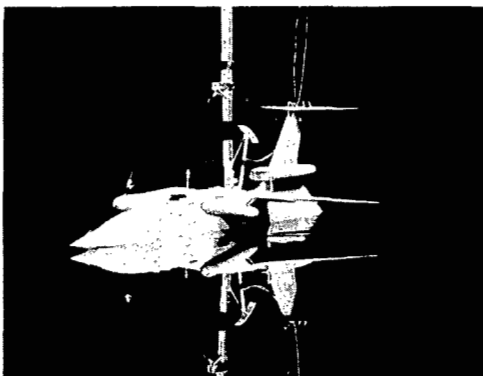
Speed, 6.6 knots
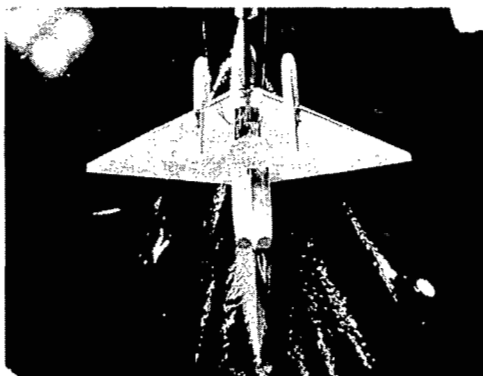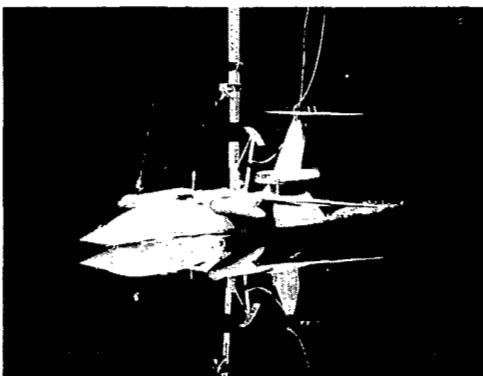
Speed, 26.5 knots
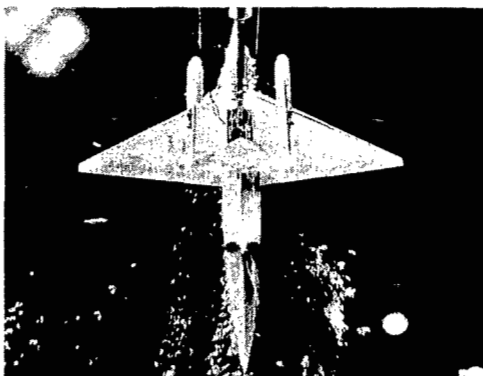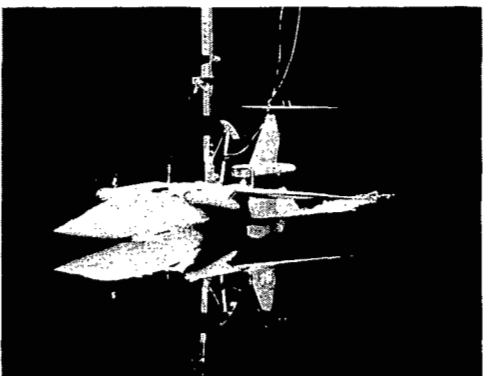
Speed, 46.3 knots

L-57-1633

Figure 23.- Spray photographs of model with power off. Gross load, 225,000 pounds.
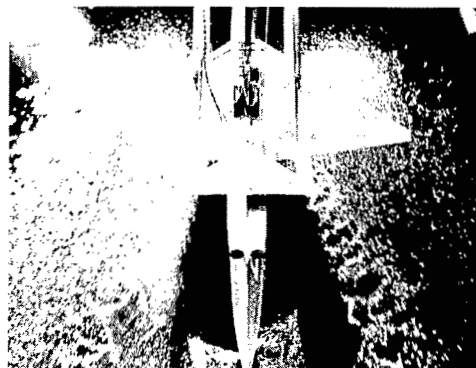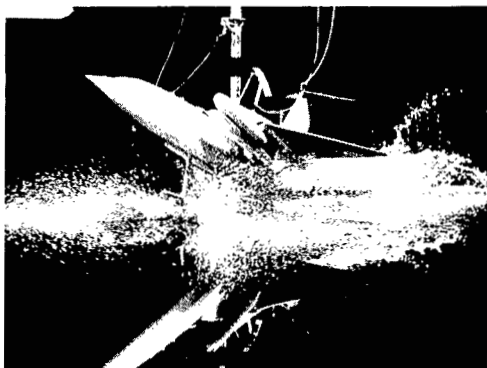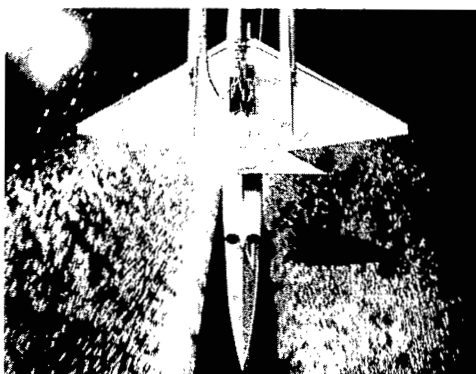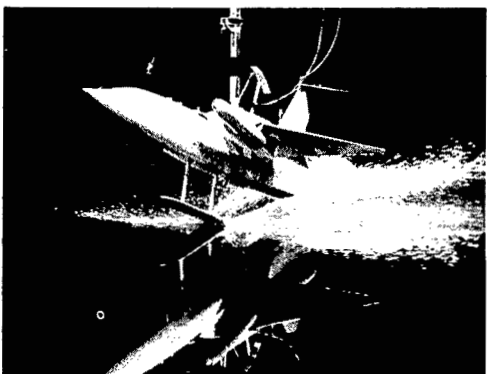
Speed, 59.6 knots
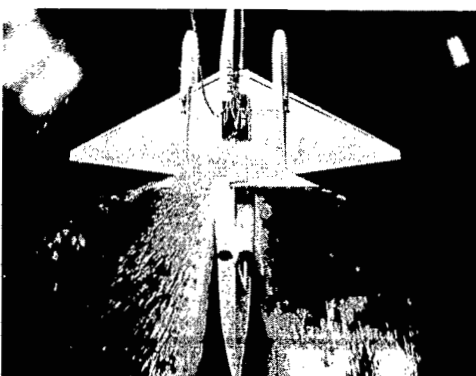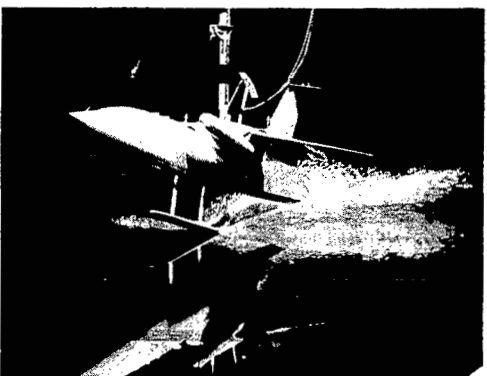

Speed, 119.2 knots

Speed, 145.6 knots

Figure 23.- Concluded.   L-57-1634
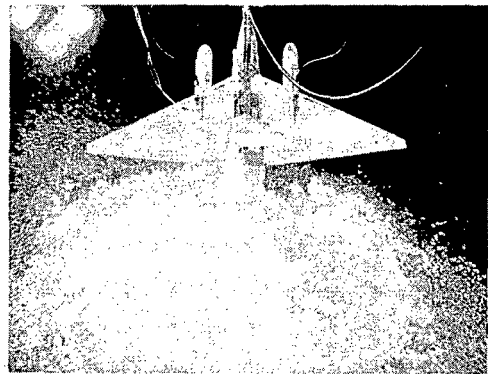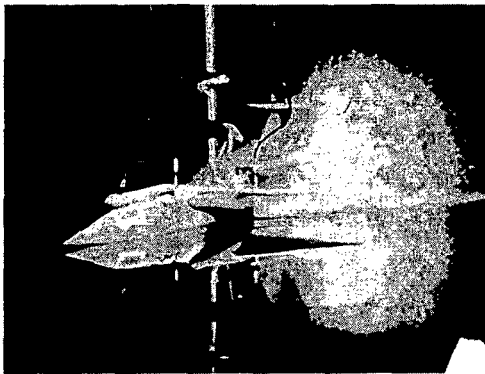
Speed, 6.6 knots
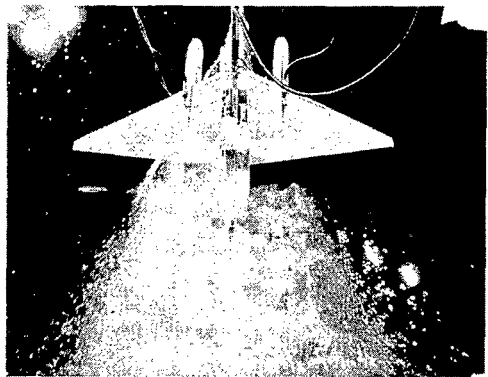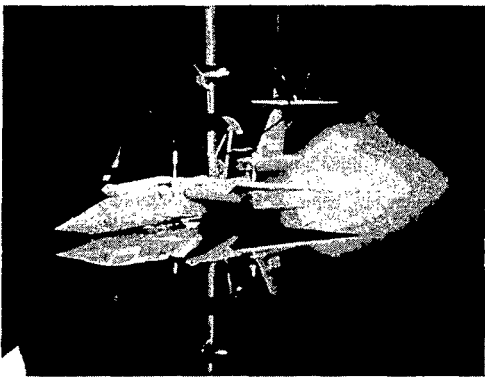
Speed, 26.5 knots
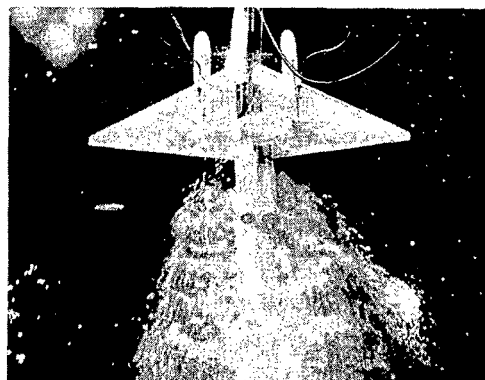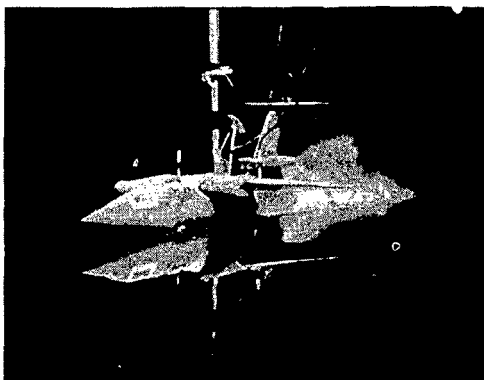
Speed, 46.3 knots

L-57-1635

Figure 24.- Spray photographs of model with power on. Gross load, 225,000 pounds.
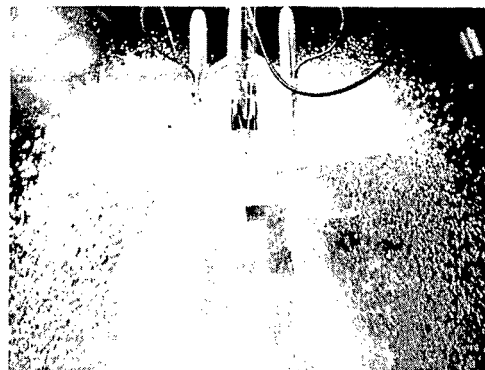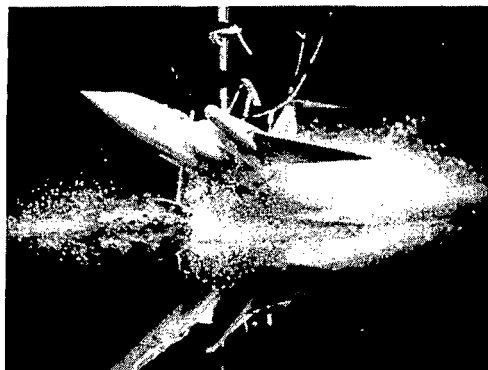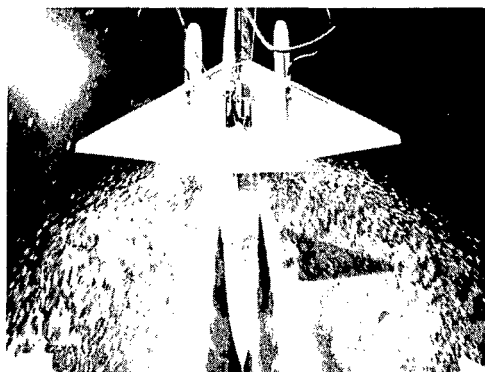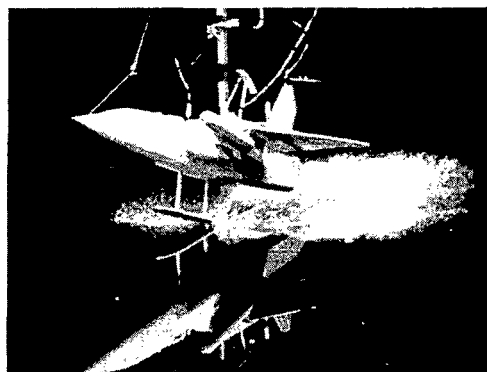
Speed, 59.6 knots
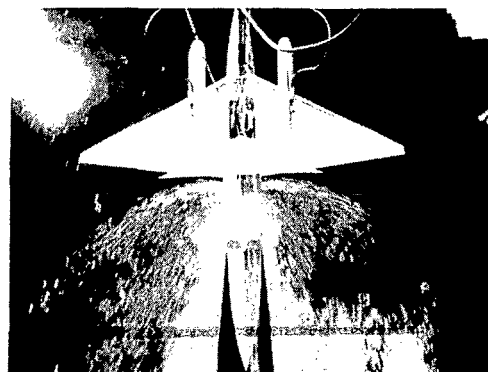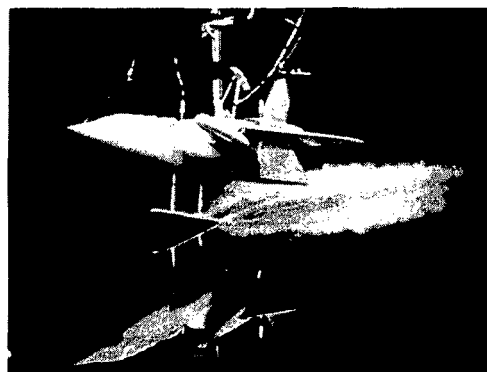
Speed, 119.2 knots

Speed, 145.6 knots

Figure 24.- Concluded.   L-57-1636
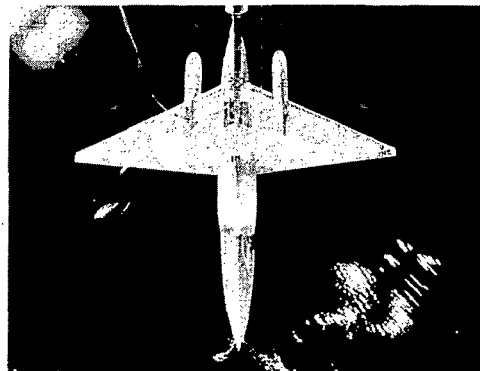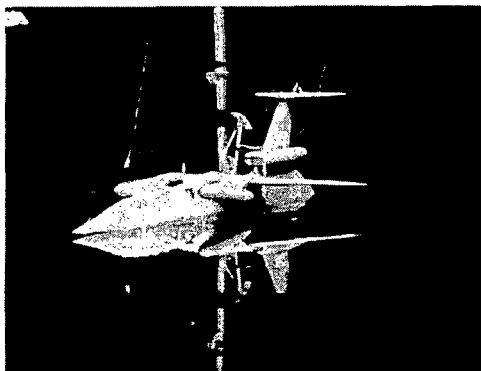
Speed, 6.6 knots
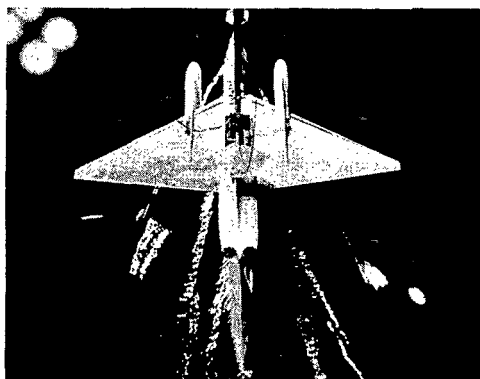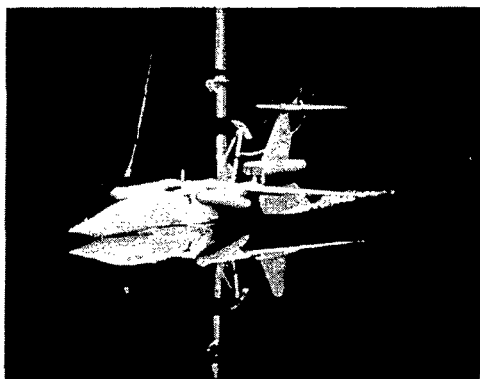
Speed, 26.5 knots
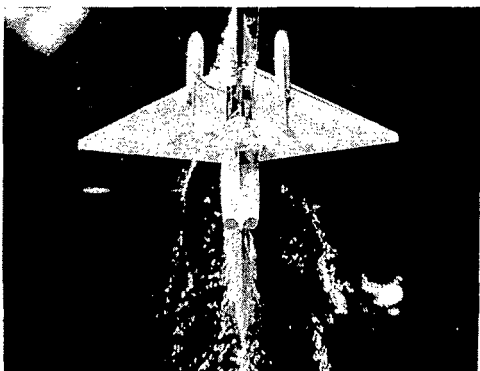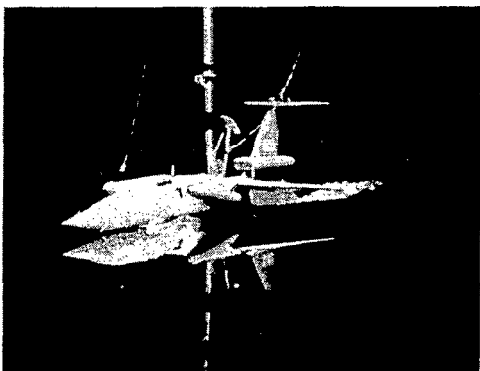
Speed, 46.3 knots

L-57-1637

Figure 25.- Spray photographs of model with power off. Gross load, 300,000 pounds.
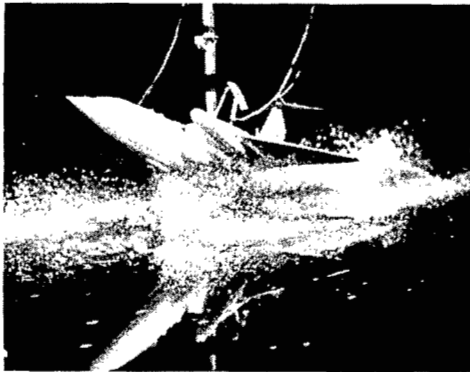
Speed, 59.6 knots
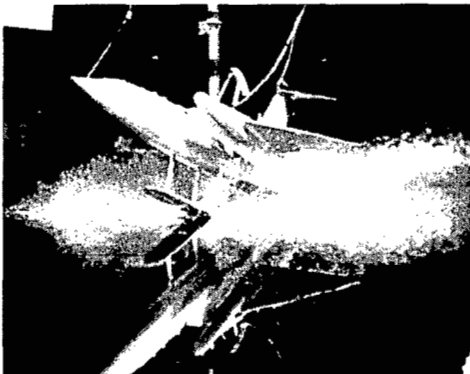
Speed, 119.2 knots
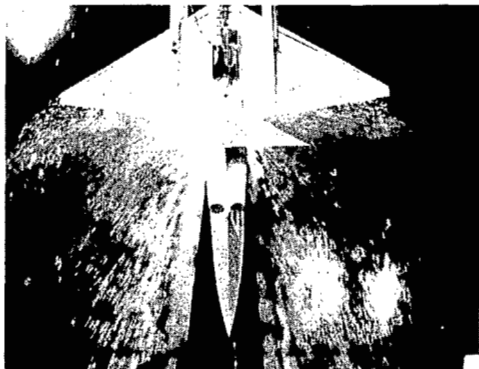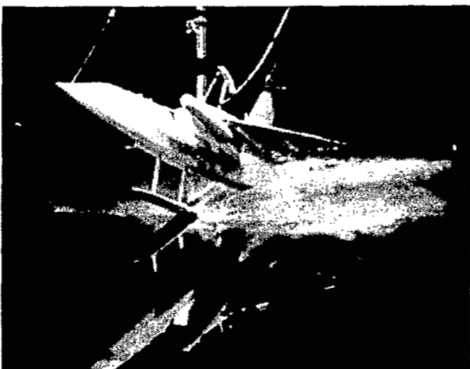
Speed, 145.6 knots

Figure 25.- Concluded.   L-57-1638
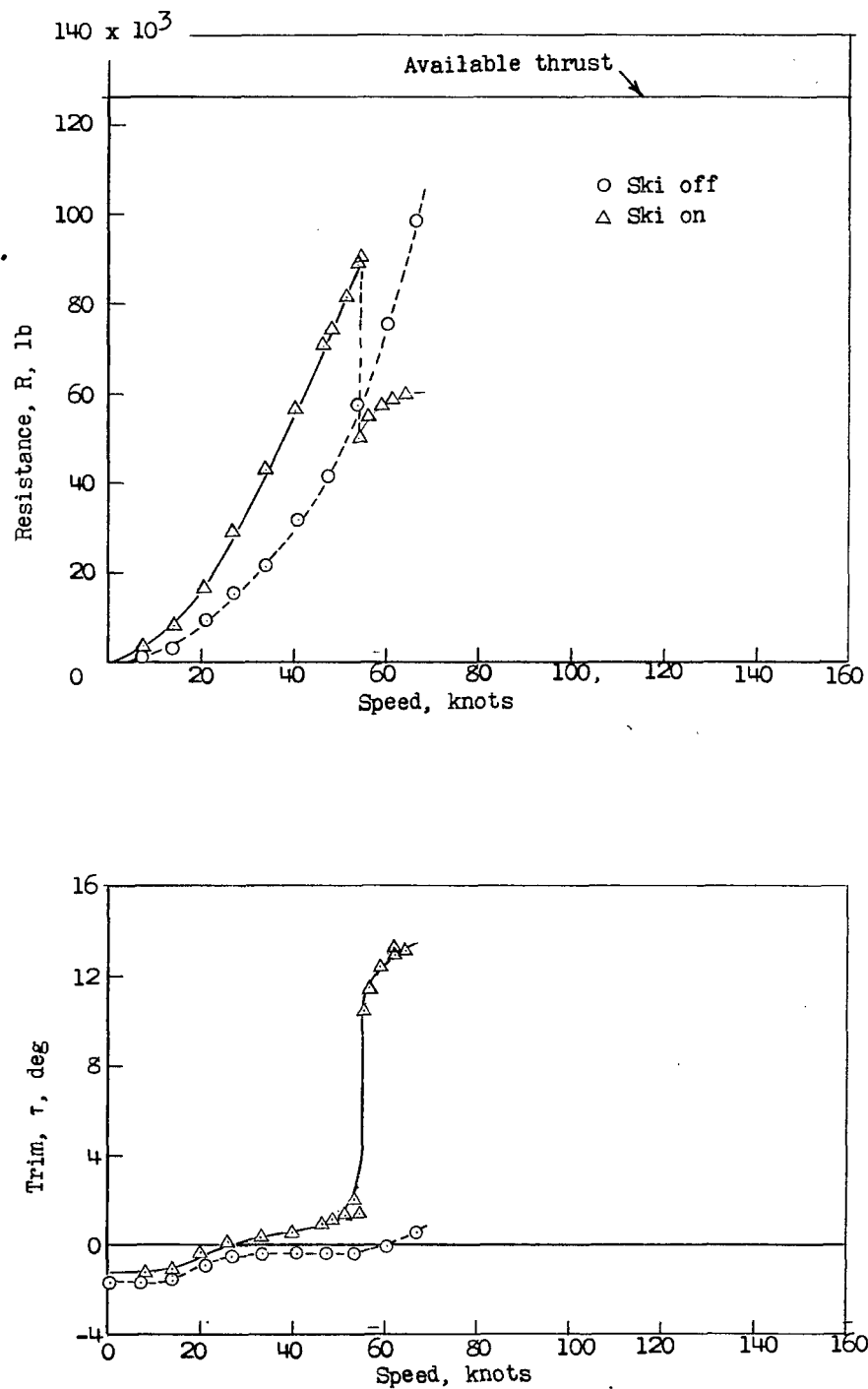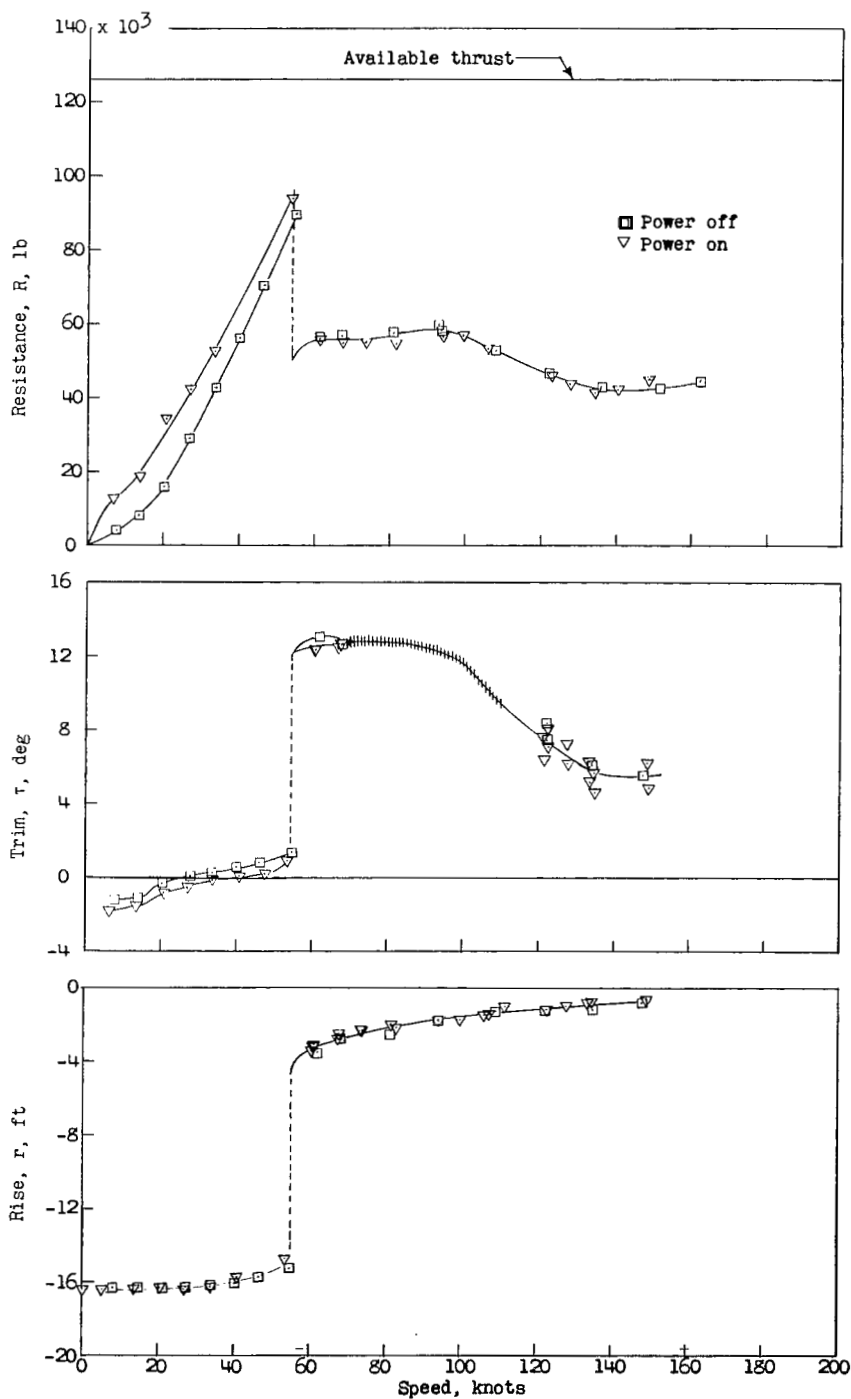
Figure 26.- Effect of removing the ski upon the resistance and trim. Gross load, 225,000 pounds; $\delta_s = -2.5^o$; $\delta_e = -5^o$.
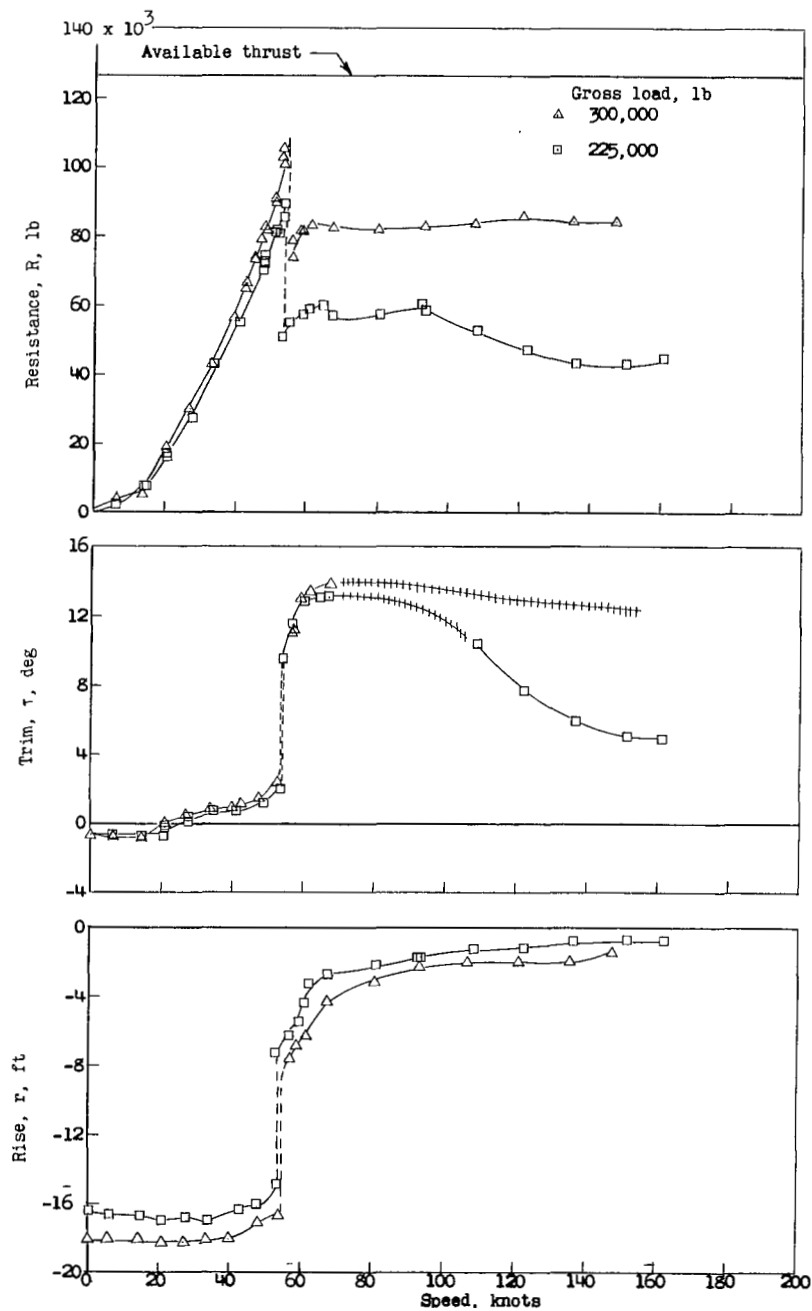
(a) Gross load, 225,000 and 300,000 pounds.

Figure 27.- Effect of gross load upon the resistance, trim, and rise. $\delta_S = -2.5^\circ$; $\delta_e = -5^\circ$.
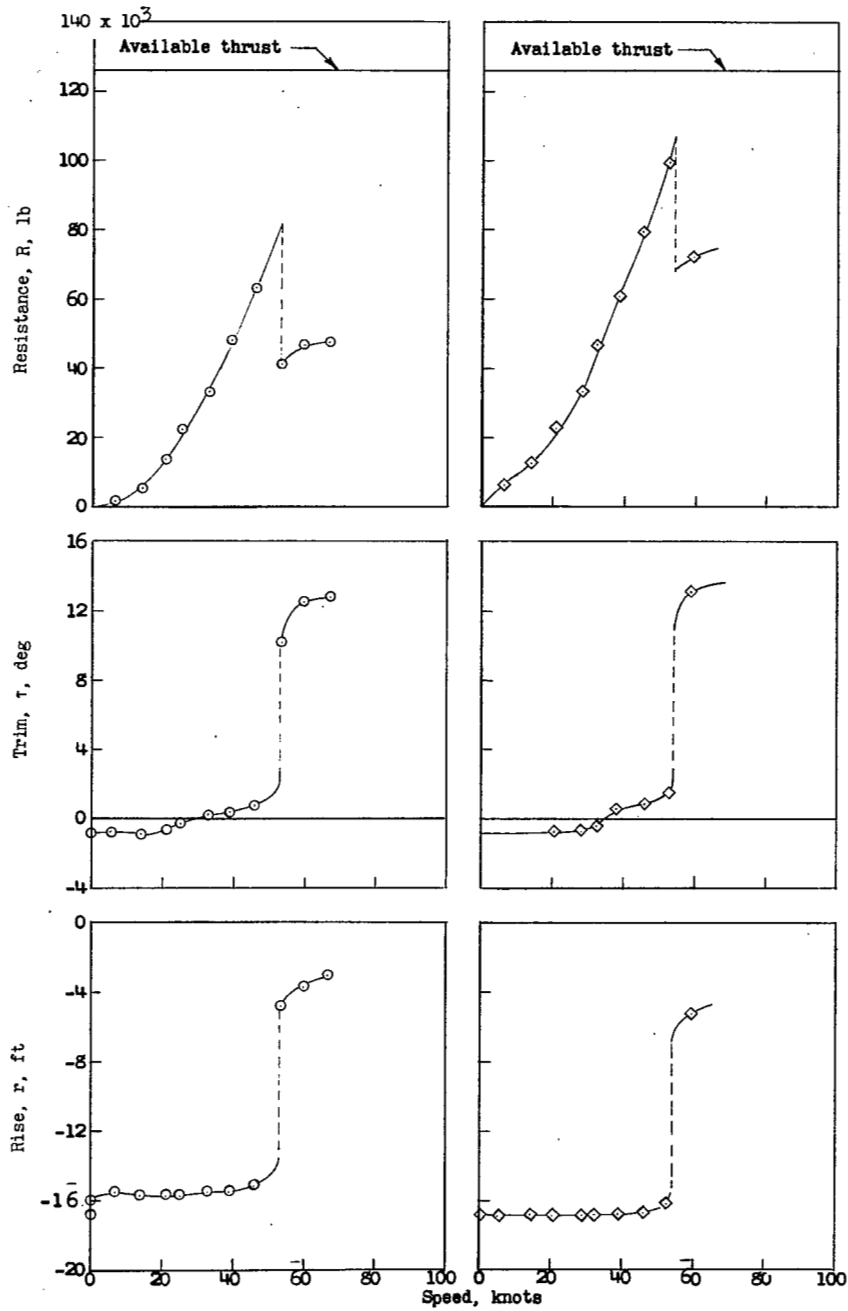
(b) Gross load, 175,000 pounds.   (c) Gross load, 250,000 pounds.

Figure 27.- Concluded.

Figure 28.- Effect of simulating the jet exhaust upon the resistance, trim, and rise. Gross load, 225,000 pounds; $\delta_s = -2.5°$; $\delta_e = -5°$.
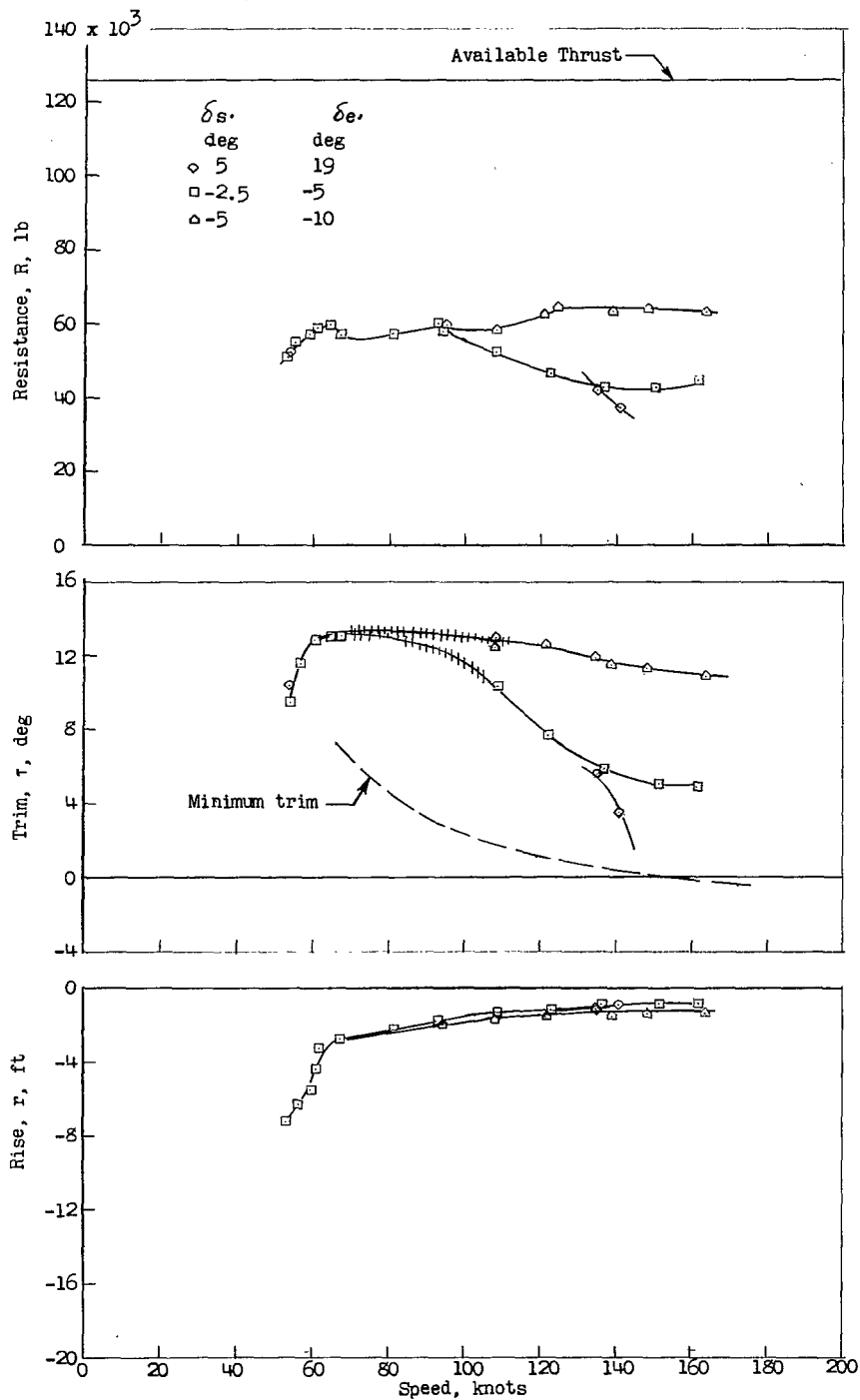
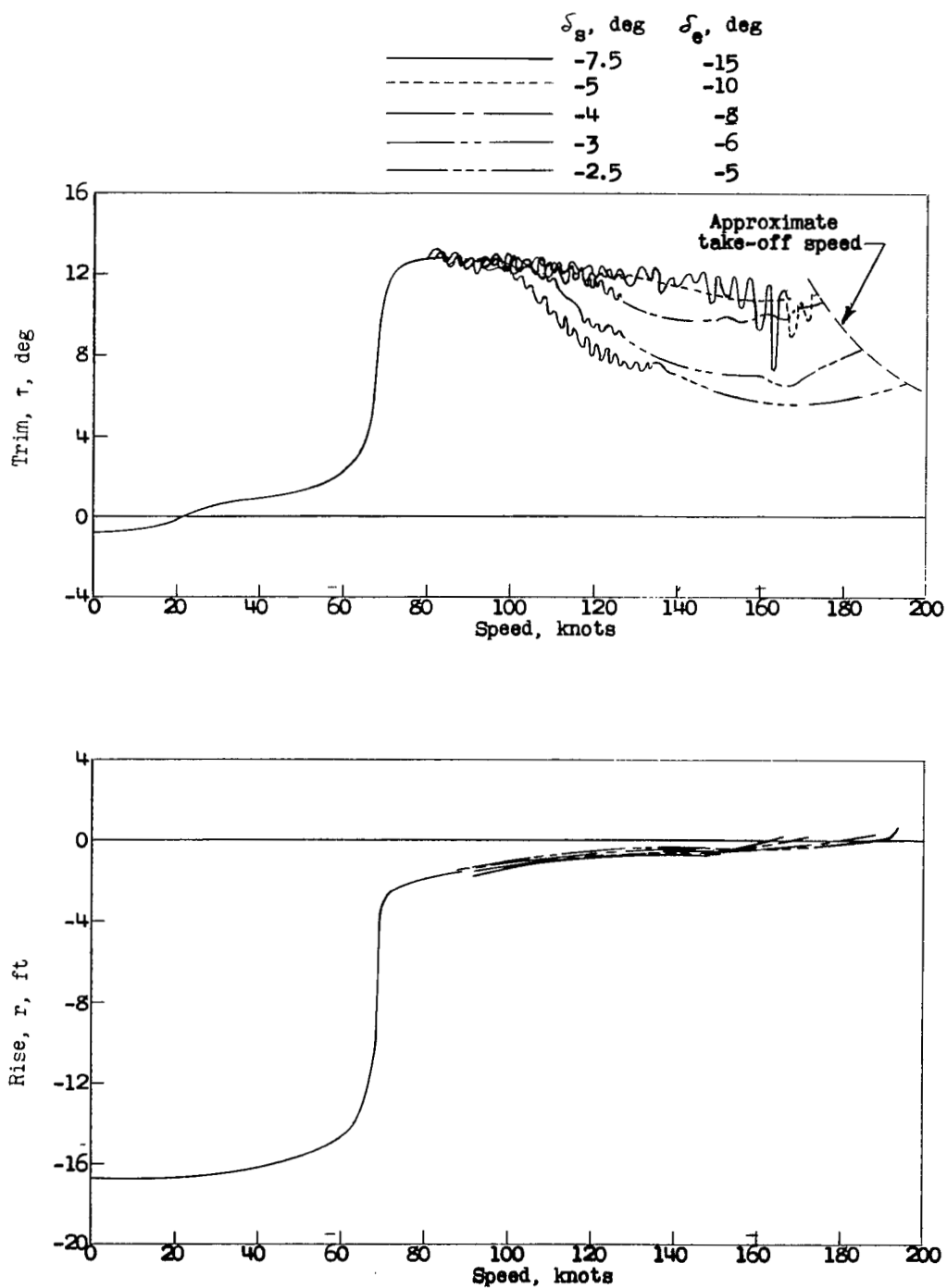Figure 29.- Effect of elevators upon the resistance, trim, and rise.
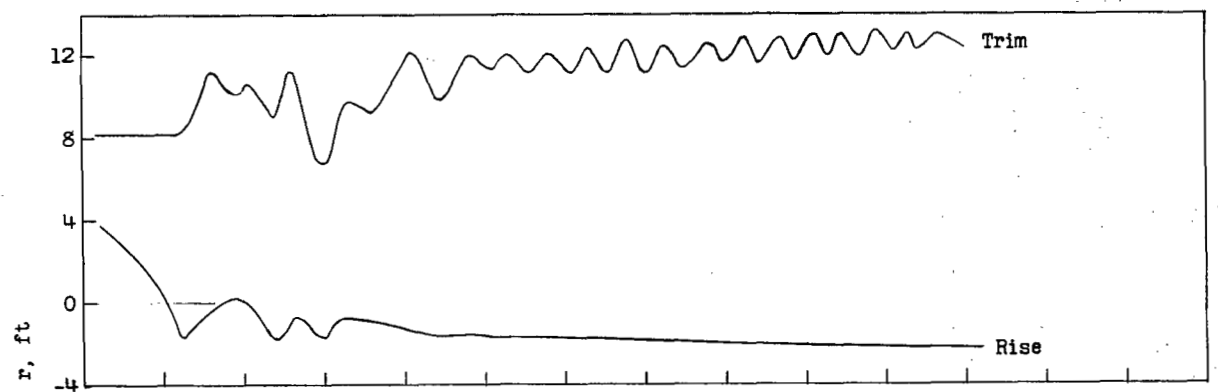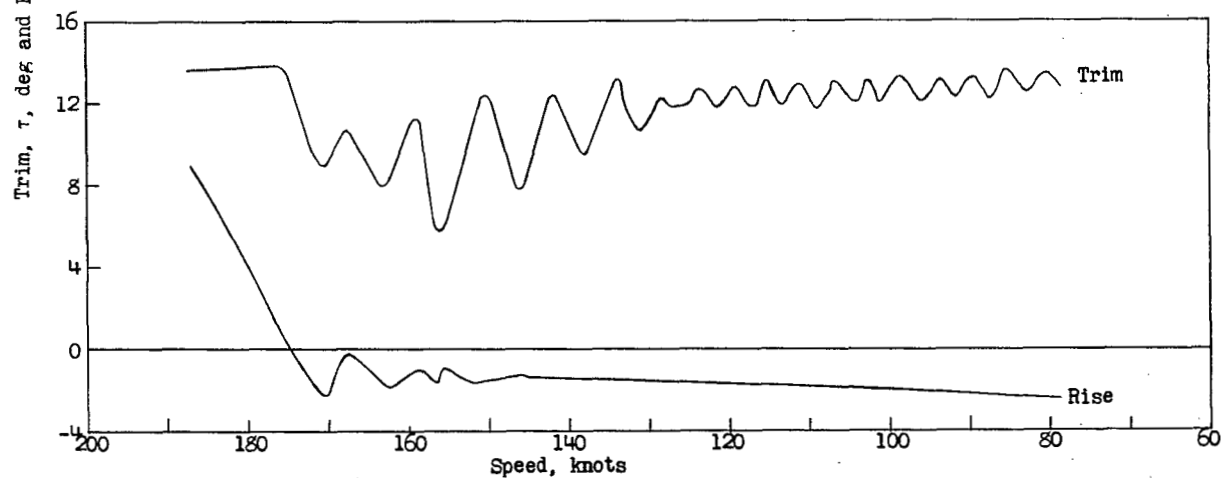Gross load, 225,000 pounds.

Figure 30.- Variation in trim and rise during smooth-water take-offs for various elevator deflections. Gross load, 225,000 pounds.

(a) Landing trim, 8.2°.

(b) Landing trim, 13.8°.

Figure 31.- Variation in trim and rise during typical smooth-water landings.